



# The role of porosity in H<sub>2</sub>/He production ratios in fracture fluids from the Witwatersrand Basin, South Africa

R. Karolytė<sup>a,\*</sup>, O. Warr<sup>b</sup>, E. van Heerden<sup>c,d</sup>, S. Flude<sup>a</sup>, F. de Lange<sup>e</sup>, S. Webb<sup>f</sup>, C.J. Ballentine<sup>a</sup>, B. Sherwood Lollar<sup>b</sup>

<sup>a</sup> Department of Earth Sciences, University of Oxford, United Kingdom

<sup>b</sup> Department of Geology, University of Toronto, Canada

<sup>c</sup> Department of Microbial, Biochemical, and Food Biotechnology, University of the Free State, South Africa

<sup>d</sup> Centre for Water Sciences and Management, North West University, Potchefstroom, South Africa

<sup>e</sup> Institute for Groundwater Studies, University of the Free State, South Africa

<sup>f</sup> School of Geosciences at the University of Witwatersrand, South Africa

## ARTICLE INFO

Editor: Dr. Don Porcelli

### Keywords:

Hydrogen  
Radiolysis  
Fracture fluids  
Precambrian basement  
Helium  
Microbial methane  
Deep carbon  
Nitrogen  
Deep subsurface life

## ABSTRACT

Abiotic H<sub>2</sub> produced in the Precambrian lithospheric crust is a key substrate at the base of the metabolic chain of chemosynthetic and photosynthesis-independent microbial communities, significant to our understanding of life on early Earth and other planets. H<sub>2</sub> cycling processes are also relevant to recent hydrogen exploration efforts and engineered subsurface environments such as radioactive waste disposal sites. In the lithospheric crust, H<sub>2</sub> is produced through water-rock reactions (serpentinisation) and radiolysis; the latter directly linked to He through radioelement decay (U, Th). The Witwatersrand Basin in South Africa is an ideal place to study the radiolytic production pathway in particular, because of the low abundance of ultramafic and mafic minerals and therefore low potential for serpentinisation reactions. Gas samples and gas flow rate data ( $n = 12$ ) were collected from the surface of exploration boreholes tapping the Witwatersrand and Ventersdorp Supergroups. The samples were predominantly composed of CH<sub>4</sub> (65–99%), N<sub>2</sub> (3–27%), He (0.1–15%), and trace amounts of C<sub>2+</sub> hydrocarbons. Notably, H<sub>2</sub> in these samples was below detection limit, despite the presence of He - providing a critical indicator of processes removing H<sub>2</sub> from the system. Using a Bayesian modelling approach, we test the hypothesis that the observed fluids are generated in-situ, driven by radioelement decay and subsequent microbial methanogenesis, and controlled by porosity of the host rock. The observed data is consistent with this hypothesis, and can be accounted for by a variation in porosity between 0.3 and 2.2% (typical values to Precambrian basement) across the different sampling sites. These He-rich hydrocarbon gases observed at the surface originate from a hydro-geological system that is porosity-constrained and isolated from externally-sourced fluids. Radioelement decay is the primary process driving the generation of H<sub>2</sub> and therefore energy production in this subsurface system, utilised by hydrogenotrophic methanogens at the base of the deep carbon cycle. Microbial utilisation is the key mechanism for H<sub>2</sub> consumptions and, conversely, preservation, suggesting that conditions favourable to commercial H<sub>2</sub> discoveries are likely constrained to hypersaline environments where microbial activity is inhibited. The model results under the proposed hypothesis (consistent N<sub>2</sub>/H<sub>2</sub> ratio between different boreholes) raises the possibility that N<sub>2</sub>, which often co-occurs with He-rich deep fluids, is also produced through radiolysis, and future work is needed to fully evaluate this hypothesis.

## 1. Introduction

Saline fracture fluids in Precambrian crystalline rocks, rich in H<sub>2</sub>, N<sub>2</sub>, He and hydrocarbons, have been shown to host diverse subsurface microbial ecosystems, including chemoautotrophic-dominated

metabolisms (Kietäväinen et al., 2017; Knipe, 1997; Lau et al., 2016; Lin et al., 2006; Lollar et al., 2019; Magnabosco et al., 2014; Pitkänen and Partamies, 2007; Telling et al., 2018; Magnabosco et al., 2018). In tectonically quiescent regions, fluid residence times in crystalline basement rocks can be on the order of thousands, to millions, and in

\* Corresponding author.

E-mail address: [ruta.karolyte@gmail.com](mailto:ruta.karolyte@gmail.com) (R. Karolytė).

<https://doi.org/10.1016/j.chemgeo.2022.120788>

Received 2 July 2021; Received in revised form 5 December 2021; Accepted 24 February 2022

Available online 2 March 2022

0009-2541/© 2022 The Authors. Published by Elsevier B.V. This is an open access article under the CC BY license (<http://creativecommons.org/licenses/by/4.0/>).

some cases even billions of years (Greene et al., 2008; Holland et al., 2013; Kietäväinen et al., 2014; Lin et al., 2006; Lippmann-Pipke et al., 2011; Lippmann et al., 2003; Warr et al., 2021, 2018), creating conditions favourable for accumulation of  $H_2$ , through a combination of processes including radiolysis (Lin et al., 2005a, 2005b; Warr et al., 2019) and hydration of ultramafic and mafic minerals (serpentinisation) (Coveney et al., 1987; McCollom and Bach, 2009), with net production rates from Precambrian crust comparable to the annual production within oceanic crust (Sherwood Lollar et al., 2014; Warr et al., 2019).  $H_2$  is a readily utilised source of energy in the subsurface by chemosynthetic autotrophs, combining  $H_2$  oxidation to reduction of electron acceptors such as  $NO_3^-$ ,  $Fe_3^+$ ,  $SO_4^{2-}$  and  $CO_2$  (Chivian et al., 2008; D'Hondt et al., 2019; Lau et al., 2016; Magnabosco et al., 2014). Radiolytic dissociation of water by energy released from radioelement decay (U, Th, K) presents a primary production pathway for elements that are incorporated in key geochemical and biological processes in the deep subsurface (Li et al., 2016; Sherwood Lollar et al., 2021). Radiolytic  $H_2$  feeds  $CH_4$  formation via both methanogenic (microbial  $CH_4$ ) production and abiotic processes including Fisher-Tropsch synthesis (Sherwood Lollar et al., 2002; Warr et al., 2020). Further, oxidants produced by radiolysis may react with dissolved species to produce electron acceptors such as  $SO_4^{2-}$  in the presence of sulphide minerals (Li et al., 2016) or organic acids in the presence of carbonates (Sherwood Lollar et al., 2021). Irradiation experiments indicate that radiolysis can play an important part in abiotic cycling of  $N_2$  through denitrification of ammonium, however current experimental verification at relevant thermodynamic conditions exists only for  $NH_3$  to  $NO_3^-$  radiolytic oxidation (Silver et al., 2012). The products of radiolysis (aqueous electrons, O and H radicals) are rapidly incorporated in other species through abiotic and biological processes, not all of which are currently well understood, and therefore rarely observed. The  $\alpha$  decay of U and Th produces radiogenic He (Ballentine and Burnard, 2002), which, in contrast to highly bioavailable radiolysis reaction products, is inert and conservative. In isolated hydrogeological systems such as the saline fluids of the Witwatersrand Basin, the He contents of the fluids thus provide a conservative tracer to evaluate the relative rates of radiolysis that occurred in the system.

Subsurface microbial communities utilise  $H_2$  through a variety of metabolic pathways dependent on the availability of electron acceptors.  $CH_4$  is a common by-product of microbial  $H_2$  utilisation in the Precambrian lithospheric crust, whether through direct methanogenesis or via acetogenesis further leading to methanogenesis (Onstott et al., 2006; Telling et al., 2018; Warr et al., 2019), the former pathway being more common (Kietäväinen and Purkamo, 2015; Lollar et al., 2019). Hydrogenotrophic methanogenesis reduces  $CO_2$ , which can be sourced from carbonate mineral dissolution, fungi assisted degradation of carbonaceous minerals (Sohlberg et al., 2015), organic material derived from weathering of metasedimentary rocks (Petsch et al., 2001) or bioavailable carbon produced via radiolysis such as acetate and formate (Sherwood Lollar et al., 2021).  $CH_4$  itself is an important energy source in the subsurface and a key intermediate component between abiotic water-rock reaction products, heterotrophic food chains, and carbon cycling in the deep subsurface (Kotelnikova, 2002). Links between radiogenic He, radiolytic  $H_2$  and hydrogenotrophic  $CH_4$  must exist, however the observed  $H_2/He$  and  $CH_4/He$  ratios in continental crust environments are highly variable (e.g. Kietäväinen et al., 2017; Sherwood Lollar et al., 2008; Warr et al., 2019) and controls on these ratios are yet not fully understood due to uncertainty in both production rates and sinks.

In this study, we investigate the effects of bulk porosity on the radiolytic, radiogenic and microbial processes governing the relationship between He,  $H_2$ ,  $N_2$  and  $CH_4$  in gas samples from boreholes tapping into Witwatersrand and Ventersdorp Supergroups in the Free State, South Africa. Bulk porosity (referred to as porosity in this paper) represents the mean fluid to rock ratio within the entire rock volume in which sampled fluids are produced in-situ and as such differs from matrix porosity (see also Holland et al., 2013; Warr et al., 2018).

The Witwatersrand Basin is particularly favourable for investigating

the relationship between radiolytic  $H_2$  and He due to the low abundance of ultramafic minerals that elsewhere in the continental lithosphere contribute an additional source of  $H_2$  (Frimmel, 2019; Lin et al., 2005a, 2005b; Sherwood Lollar et al., 2014). Deep crustal lithospheric hydrogeological systems are rarely accessible, therefore developing models for the primary chemical and microbial processes which can be extrapolated from geochemical and proxy signals at the surface is extremely important for exploration of deep subsurface ecosystems on Earth and other planets, as well as commercial utilisation of naturally occurring He and  $H_2$ .

This paper combines methods for He and  $H_2$  production calculations (Ballentine and Burnard, 2002; Blair et al., 2007; Lin et al., 2005a, 2005b; Warr et al., 2019) to investigate the effects of abiotic parameters on the observed  $CH_4/He/N_2$  budgets and to evaluate evidence for hydrogenotrophic methanogenesis using a Bayesian modelling approach.

## 2. Geological background

The Witwatersrand Basin is located at the centre of the Kaapvaal Craton which formed during a series of discrete pulses of tectonomagmatic activity between 3.074 and 2.642 (Cornell et al., 2021; Robb and Meyer, 1995), overlain by the Ventersdorp andesitic volcanic extrusive sequence at 2.7 Ga (Coward et al., 1995). The setting is one of the best preserved Archean basins in the world and an active site of ore mining, primarily of gold and uranium (Frimmel, 2019). Major thermal perturbations include the emplacement of the Bushveld complex at 2054 Ma (Robb et al., 1997) and the Vrederfort impact event at 2020 Ma (Kamo et al., 1996). The samples for this study were collected from exploration boreholes located on the south-western margin of the basin, within 20 km of Welkom in the Free State (Fig. 1). Mining is predominantly targeting ore zones within the quartzites of the Witwatersrand Supergroup, which dip to the northeast. The Ventersdorp Supergroup overlies the Witwatersrand Supergroup in the northern part of the region. The Karoo Supergroup unconformably overlays both strata, comprising fluvial sedimentary lithologies and occasionally dissected by Karoo dykes (Onstott et al., 2006 and references therein). Numerous deep exploration boreholes provide access for sampling deep fluids at high flow rates that have lasted for decadal timescales. Many of these legacy gas mineral exploration boreholes had unexpectedly high gas flows and were capped due to dangerously high emission rates. High gas flow rates correspond to crustal fracture zones, trending N-S and E-W. Gas emissions (primarily  $CH_4$ ) are encountered in underground mining and present a significant safety and mine explosion hazard (Mkhabela and Manzi, 2017).

### 2.1. Sampling methods

Gas samples were collected from 12 uncased boreholes drilled to depths between 514 and 1750 m, tapping into the Witwatersrand and Ventersdorp Supergroups. Sampling was undertaken at the borehole collars at the surface using a method described in (Sherwood Lollar et al., 2002; Ward et al., 2004). Plastic tubing was attached to the end of the packer and the flow of water from the borehole was directed into an inverted graduated funnel. Borehole gas was flowed through the tubing long enough to displace any air remaining in the borehole or the equipment before sampling (typically  $10\times$  the volume of tubing). Collected gases were then transferred into pre-evacuated vials using a needle on a Luer attachment at the top of the beaker. Vials were prefixed with saturated  $HgCl_2$  solution to prevent microbial activity in the vials post-collection after the methods of Oremland (1988). In 2007, gas flow meters were installed in 12 boreholes for continuous flow measurement over a period of 14 consecutive months. This included 4 additional boreholes that were not sampled for major gas concentration analysis, and another 4 boreholes sampled for major gas concentrations were not monitored for gas flow rate (full summary of data types available for

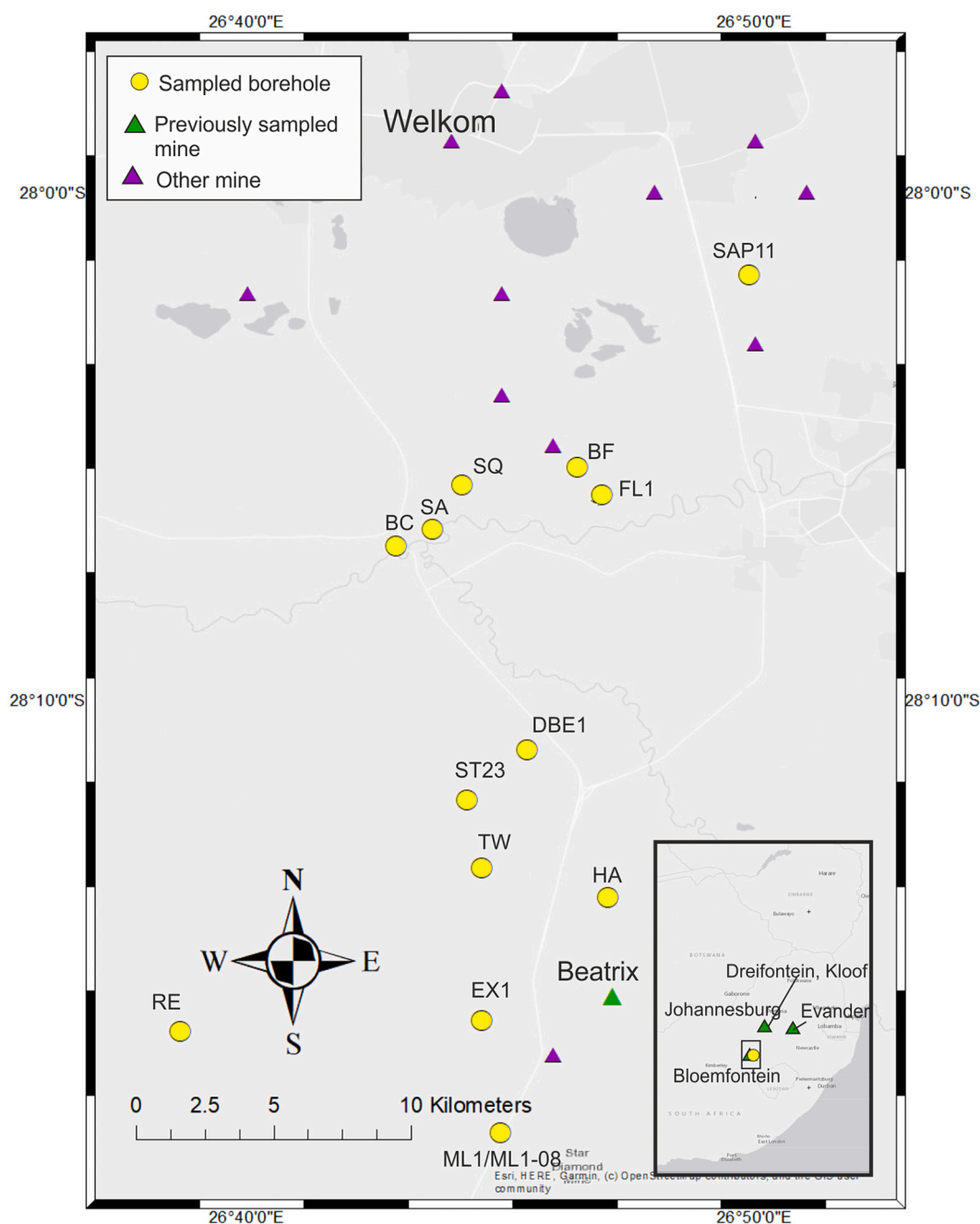


**Fig. 1.** Map showing the locations of sampled boreholes in the vicinity of Welkom, Free State, South Africa. The sampled sites (yellow circles) are surface exploration boreholes. Previously sampled mines (Lippmann-Pipke et al., 2011; Lippmann et al., 2003; Sherwood Lollar et al., 2008, 2006; Ward et al., 2004) are shown for reference (green triangles). (For interpretation of the references to colour in this figure legend, the reader is referred to the web version of this article.)

each borehole is in Table S1). Methane concentrations were also measured monthly over a 5-month period in 2008, using a hand-held meter to monitor the temporal gas composition fluctuations on a subset of boreholes.

## 2.2. Compositional and isotopic analysis

Compositional analyses of gas samples were performed at the Stable Isotope Laboratory at the University of Toronto. A Varian 3400 GC equipped with a flame ionization detector (FID) was used to determine concentrations of C<sub>1</sub>-C<sub>4</sub> hydrocarbons, while a GC equipped with TCD was used for concentrations of the inorganic gas components (H<sub>2</sub>, He, Ar, O<sub>2</sub>, CO<sub>2</sub> and N<sub>2</sub>). Reproducibility of major gas concentrations was

±5%. The reported bulk gas concentrations are corrected for air contamination during sampling, as previous work has established that the saline fluids are highly reducing with no detectable natural O<sub>2</sub> levels (Sherwood Lollar et al., 2006). Analyses for δ<sup>13</sup>C values were performed by continuous flow compound specific carbon isotope ratio mass spectrometry with a Finnigan MAT 252 mass spectrometer. The total error incorporating both accuracy and reproducibility is ±0.5‰ with respect to V-PDB standard (Sherwood Lollar et al., 2007). The δ<sup>2</sup>H analysis was performed on a continuous flow Finnigan MAT delta<sup>+</sup>-XL isotope mass spectrometer that consists of an HP 6890 gas chromatograph, with a total uncertainty of ±5‰ with respect to V-SMOW (Sherwood Lollar et al., 2007).

### 3. Results and discussion

#### 3.1. Gas flow rate

Gas flow rate was relatively constant in the majority of monitored boreholes, with an exception of the first month of sampling, where recorded gas flow was 60%–360% higher than the mean flow rate within the whole observation period. As this may represent a sampling artefact, data from this first time point were excluded from the following analysis. The median flow rate during the observation period was  $2 \times 10^6$  L/day per borehole. This results in a total of  $1.4 \times 10^{11}$  L of gas emitted from all boreholes over the ~ one year observation period. The gas flow rate was generally consistent within individual boreholes, with standard deviation between monthly readings within 3–9%, with an exception of 4 boreholes where gas flow readings varied more significantly (Fig. 2). CH<sub>4</sub> concentrations were measured with a hand-held meter monthly between March and July 2008 (Table S2). CH<sub>4</sub> concentrations remained stable within 2–4% between different sampling times and were in agreement with concentration measurements carried out later in the laboratory by GC. Major gas concentrations and stable isotope ratios from discrete samples collected for GC and mass spectrometry measurements are representative of the gases emitted through the period of observation time.

#### 3.2. Major gas geochemistry

The samples were predominantly composed of CH<sub>4</sub> (65–99%), N<sub>2</sub> (3–27%) and He (0.1–15%), with an exception of sample SQ which does not contain N<sub>2</sub> (Fig. 3). H<sub>2</sub> was below detection limit in all borehole samples (<0.01%) (Table S3). He concentrations are significantly higher than the current economic threshold for He production from sedimentary basins (>0.3%) (Bare et al., 2016), and comparable to recent discoveries in Tanzania (Danabalan, 2017). The last episode of volcanic activity within the basin was during late Archean to early Proterozoic (Bowen et al., 1986) and previously recorded <sup>3</sup>He/<sup>4</sup>He ratios in deep fluids are within the crustal He range (0.0015–0.04 R/Ra) (Heard et al., 2018; Lippmann-Pipke et al., 2011; Lippmann et al., 2003), so mantle He contribution is discounted. Radiogenic <sup>4</sup>He produced in the crust by  $\alpha$  decay of <sup>235,238</sup>U and <sup>232</sup>Th is typically directly proportional to the concentrations of these elements, which are most concentrated in accessory minerals (Ballentine and Burnard, 2002). With the average He production rate of  $2.9 \times 10^{-11}$   $\mu$ M/year per gram of rock, using average

U/Th concentrations in the upper crust (Rudnick and Fountain, 1995), either long residence times in tectonically quiescent regimes, or fluid mobilisation and secondary migration over long distances are required to account for these concentrations (Ballentine and Sherwood Lollar, 2002). Though migration cannot be ruled out, fracture water flow rates in crystalline rock basements are typically low (Kloppmann et al., 2002; Warr et al., 2019), and noble gas residence times in the fracture fluids in the Witwatersrand Basin are typically in the range of thousands, and up to hundreds of millions of years (Borgonie et al., 2019; Heard et al., 2018; Lippmann et al., 2003). Helium is highly diffusive and reaches equilibrium between host mineral and pore fluids within tens of thousands of years (at ambient temperature) (Tolstikhin et al., 2011; Rufer et al., 2018). Over fluid residence times quoted above, virtually all He will likely be partitioned into the pore fluids. Low hydraulic conductivity and low porosity in these fractured rock hydrogeologic environments suggest that long-term in-situ accumulation over geological periods of time is the more likely cause of these observed He concentrations (Sherwood Lollar et al., 2014).

He/N<sub>2</sub> ratios in the sample suite range between 0.2 and 1.4, with two exceptions: SQ which does not contain N<sub>2</sub>, and FL1 with an exceptionally low He/N<sub>2</sub> ratio of 0.01. He concentrations in this sample are 0.1%, more than an order of magnitude lower than the median value observed in the other boreholes (5.6%), suggesting preferential He loss, which could have occurred either naturally or during sampling. The range of He/N<sub>2</sub> ratios observed in the present study fall within the distribution and close to the median value (0.23) observed in previous fracture fluid studies from the Witwatersrand Basin (Fig. 4) (Heard et al., 2018; Onstott et al., 2006; Sherwood Lollar et al., 2006; Ward et al., 2004), suggesting a common source. High N<sub>2</sub> concentrations are commonly associated with high He (Ballentine and Sherwood Lollar, 2002). Nitrogen species (NH<sub>4</sub>, NH<sub>3</sub>, NO<sub>3</sub><sup>-</sup>, NO<sub>2</sub><sup>-</sup>, N<sub>2</sub>) are introduced to subsurface fluids through the devolatilisation of NH<sub>4</sub><sup>+</sup> in silicates, thermal decomposition of organic matter, release of fluids in mineral inclusions and microbial cycling (Doane, 2017). In a tectonically quiescent setting, the kinetics of low-temperature devolatilisation reactions, which occur at ambient and metamorphic temperatures (20–900 °C) (Li et al., 2009; Li et al., 2012 and references therein), may be the primary control of N species transfer from solid to aqueous state (Li et al., 2021). In Witwatersrand basin lithologies specifically, N species primarily exist as NH<sub>4</sub><sup>+</sup> within the phyllosilicate mineral structure and NH<sub>3</sub>/NH<sub>4</sub><sup>+</sup> in fluid inclusions (Silver et al., 2012). In solution, multiple abiotic pathways exist for N<sub>2</sub> production from the N species, including further thermal decomposition and radiolytic reactions (Doane, 2017). Much more is known about microbiological cycling of N species. Denitrification is driven by microbial cycling (Granger et al., 2008) with evidence for a complete metabolic pathway to N<sub>2</sub> discovered in the deep subsurface environments globally (Sheik et al., 2021). N<sub>2</sub> production is likely a result of a combination of all of these processes and the relative importance of each remains an active area of research. N<sub>2</sub> concentrations in fluids ultimately are likely to be strongly controlled by the composition of phyllosilicates and the kinetics of nitrogen cycling in the subsurface, therefore a range of He/N<sub>2</sub> ratio values between different sampling sites is expected. Sample SQ is the only sample which does not contain N<sub>2</sub> but does contain He concentrations comparable to those in the other boreholes, which may suggest a larger abiotic and/or microbial N<sub>2</sub> sink in the borehole relative others.

#### 3.3. The occurrence of methane and its dependency on hydrogen

Hydrocarbon species are primarily dominated by CH<sub>4</sub> with trace amounts of C<sub>1</sub>–C<sub>4</sub> hydrocarbons (Table S4). CH<sub>4</sub> isotopic ratios are relatively depleted in <sup>13</sup>C and enriched in <sup>2</sup>H, with most samples giving values that are commonly associated with microbial CO<sub>2</sub> reduction (Fig. 5a), a plausible CH<sub>4</sub> source also consistent with high C<sub>1</sub>/C<sub>2+</sub> ratios (1108–40,850) (Fig. 5b). The wider literature of Witwatersrand basin fracture fluid gases investigated over the past few decades indicates a

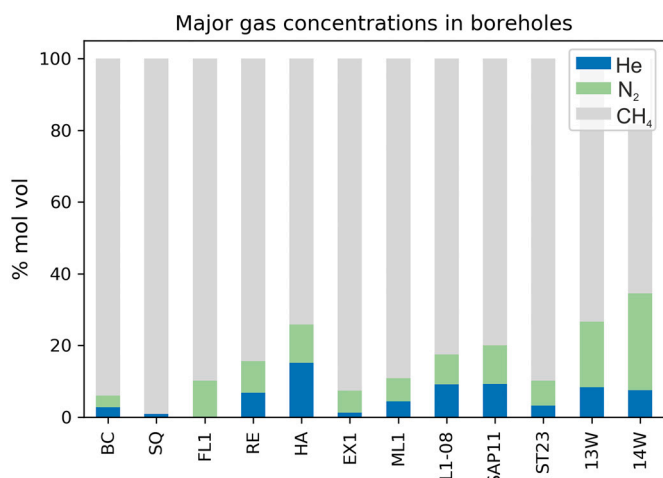


Fig. 2. Major gas concentrations in sampled boreholes. The dominant gas species are CH<sub>4</sub>, N<sub>2</sub> and He. The relative gas mass balance is highly varied between different boreholes: CH<sub>4</sub> varies between 65 and 99%; N<sub>2</sub> 3–27%; He 0.1–15%. Trace amounts of C<sub>2</sub>–C<sub>4</sub> hydrocarbons are present and not plotted (see Table S2).



### Timeseries of flowrate in boreholes

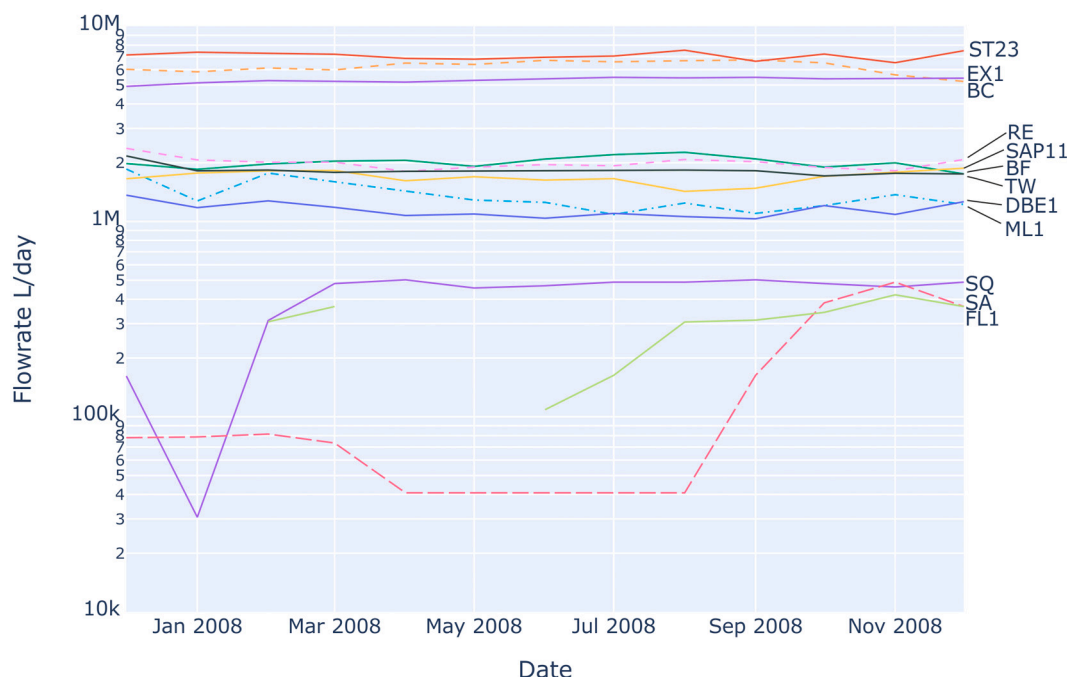


Fig. 3. Gas flowrate (in L/day) in observation boreholes from November 2007 through to December 2008.

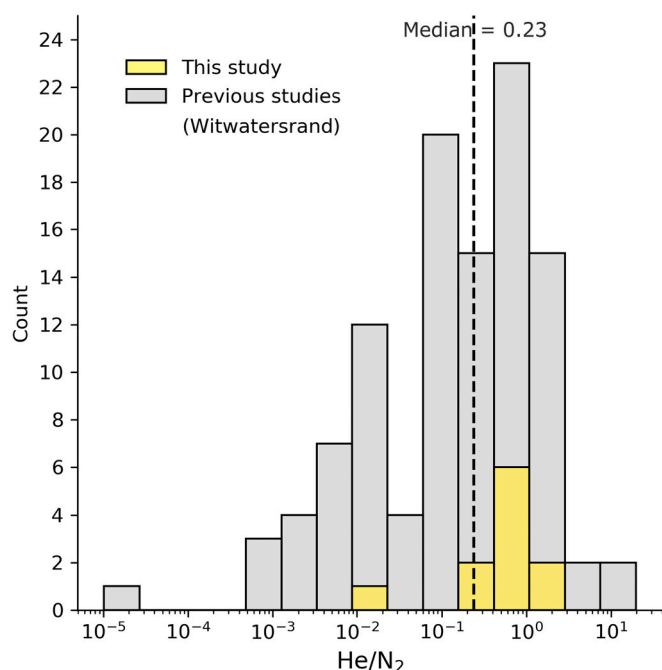
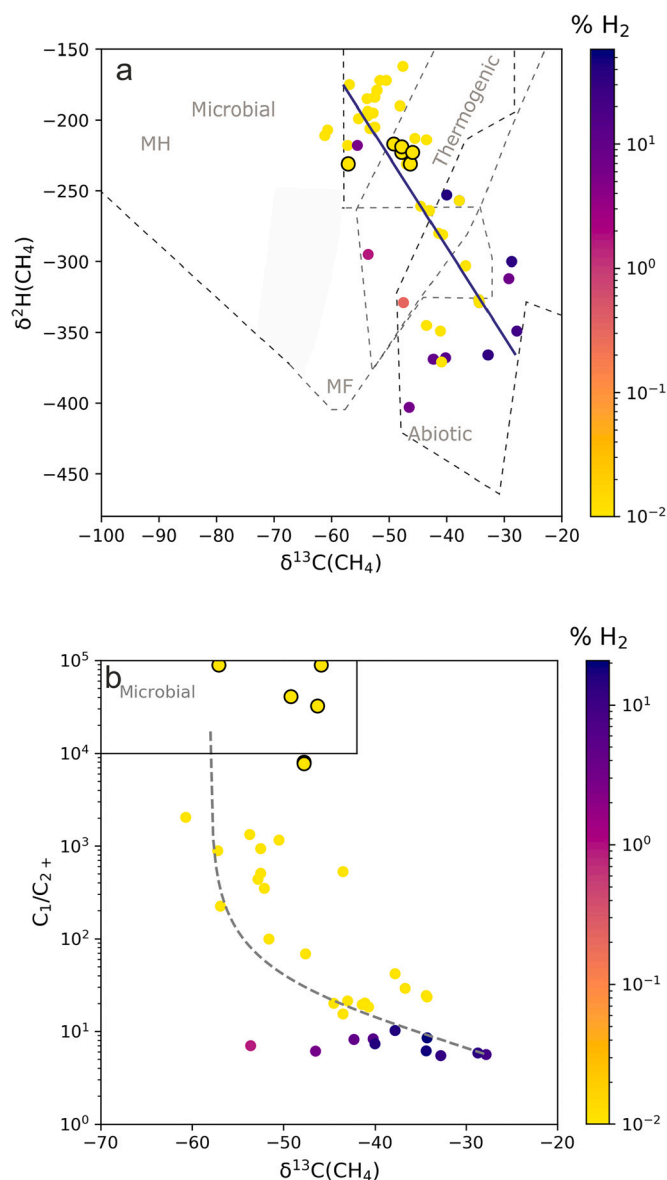


Fig. 4. Histogram of  $\text{He}/\text{N}_2$  ratios from this study ( $n = 12$ ) compared to previously reported data from fracture fluids in Witwatersrand Basin (Heard et al., 2018; Onstott et al., 2006; Sherwood Lollar et al., 2006; Ward et al., 2004). The observed  $\text{He}/\text{N}_2$  ratios are consistent with the regional median value (0.23) of deep fracture water samples, suggesting a common source and no significant secondary fractionation.

range of  $\text{CH}_4$  sources from other sites, from microbial-dominated  $\text{CH}_4$ , to signatures characteristic of abiotic end-members (Sherwood Lollar et al., 2006, 2008). In addition to stable isotope composition of  $\text{CH}_4$ , previous studies demonstrated evidence for abiotic origin of some of these gases

based on  $\delta^{13}\text{C}$  and  $\delta^2\text{H}$  patterns in  $\text{C}_2\text{-C}_5$  alkanes, reaction spectrum characterisation as well as hydrogeological and geological context (Etiope and Sherwood Lollar et al., 2002, 2008, 2006; Warr et al., 2021). Samples from the previous studies lie on binary mixing trend between microbial and abiotic end-members (the former include Beatrix, Evander, Masimong (Ward et al., 2004; Sherwood Lollar et al., 2008; Simkus et al., 2016), the latter Mponeng mine (Sherwood Lollar et al., 2006) (Fig. 5). The samples presented here plot close to the microbial end-member.

Within the  $\text{CH}_4$  stable isotope distribution of previously reported fracture fluids from the Witwatersrand Basin, samples with abiotic signatures in  $\text{CH}_4$  isotope ratios are often associated with the highest concentrations of  $\text{H}_2$  (Sherwood Lollar et al., 2006) (Fig. 5).  $\text{H}_2$  has a high enzymatic potential as a key electron donor (pairing with a wide range of electron acceptors) for chemosynthetic microbial communities present in fracture water and deep sea sediments (Lau et al., 2016; Lin et al., 2006; Magnabosco et al., 2014; Sauvage et al., 2021).  $\text{H}_2$  therefore does not accumulate to high concentrations compared to less bioavailable crustal fluids, such as  $\text{He}$  and  $\text{N}_2$ , unless microbial metabolisms are inhibited by other environmental factors such as salinity (Telling et al., 2018) or other substrate limitations (Lin et al., 2006; Lollar et al., 2019). Hydrogenotrophic methanogens (Takai et al., 2001; Ward et al., 2004) and methane oxidisers (Gihring et al., 2006; Lau et al., 2016; Magnabosco et al., 2014; Simkus et al., 2016) have been detected in multiple sites across the Witwatersrand Basin at depths between 0.7 and 3 km. The absence of  $\text{H}_2$  and abundance of microbial  $\text{CH}_4$  in some systems is consistent with hydrogenotrophic microbial communities changing the proportion of  $\text{H}_2$  relative to  $\text{CH}_4$  in these fluids. The scarcity of radiolytic  $\text{H}_2$  due to rapid microbial utilisation has been previously observed in subsurface marine (D'Hondt et al., 2009, 2019) and continental settings (Ward et al., 2004; Sherwood Lollar et al., 2006). Methanogens exhibit the highest growth rate between 40 and 50 °C and can survive up to 80 °C (Doerfert et al., 2009), at pH values between 4 and 8 (Zinder, 1993). Given the low geothermal gradient in the Witwatersrand basin (10 °C/km (Omar et al., 2003), the optimal window is at 2.5–3.5 km depth, but can potentially extend to 6 km depth. While fluid samples



**Fig. 5.** a)  $\delta^{13}\text{C}$  vs  $\delta^2\text{H}$  of  $\text{CH}_4$  plot showing the empirically determined fields of gas origin (Etioppe and Sherwood Lollar, 2013) adapted from (Schoell, 1988). Abbreviations indicate: MH – hydrogenotrophic methanogenesis; MF – microbial acetate fermentation. The solid line shows an example of a theoretical mixing between abiotic and microbial end-members. b) Plot of  $\delta^{13}\text{C}_{\text{CH}_4}$  values versus  $\text{CH}_4/\text{C}_{2+}$  ratios. Microbial field from (Etioppe and Sherwood Lollar, 2013; Hunt, 1996). Circles with black edges are data from this study, smaller circles are from a literature compilation of fracture fluids in Precambrian basement rocks from the Witwatersrand Basin (Sherwood Lollar et al., 2006; Simkus et al., 2016; Ward et al., 2004). Symbol colour indicates sample hydrogen concentrations. Samples with  $\text{H}_2$  concentrations below detection limit (typically  $<0.01\%$ ) are also displayed in colour at the bottom of the colour bar (yellow). Dashed line shows a hypothetical mixing relationship between microbial and abiotic end-members as discussed in the main text. (For interpretation of the references to colour in this figure legend, the reader is referred to the web version of this article.)

from this dataset were unavailable, pH values reported in fracture waters from mine samples were  $8.2 \pm 0.5$  pH (Magnabosco et al., 2014), suitable for methanogenesis.

Methanogenesis typically requires a stoichiometry of 4  $\text{H}_2$  molecules to produce one  $\text{CH}_4$  molecule, a ratio that is the same for both microbial and abiotic methanogenesis (full reaction list in Warr et al., 2019). Converting the measured  $\text{CH}_4$  contents to  $\text{H}_2$  using a 1:4 ratio and

neglecting other  $\text{H}_2$  sinks (other microbial  $\text{H}_2$  utilisation and  $\text{H}_2/\text{He}$  diffusion) gives a first order  $\text{H}_2/\text{He}$  production range of 19–411. These values overlap with estimates similarly calculated for the theoretical upper and middle continental crust (15–117) by Sherwood Lollar et al. (2014), with two outliers. While the overwhelming isotopic evidence supports primarily microbial  $\text{CH}_4$  origin at the specific sites investigated in this study (Fig. 5a), minor abiotic component is also taken into account by this conversion (Warr et al., 2019), however it is likely to be negligible. Where abiotic hydrocarbons are dominant, high concentrations of  $\text{C}_{2+}$  hydrocarbons produced from abiotic  $\text{CH}_4$  polymerisation are often observed (e.g. Sherwood Lollar et al., 2002; Sherwood Lollar et al., 2006). At the sites discussed here, concentrations of  $\text{C}_{2+}$  hydrocarbons are negligible (up to 0.06%, Table S3), suggesting that abiotic signatures are overwhelmed by a much larger microbial hydrocarbon (principally  $\text{CH}_4$ ) component, in line with previous observations (Sherwood Lollar et al., 2006; Simkus et al., 2016; Ward et al., 2004).

One possible explanation of this apparent variability in  $\text{H}_2/\text{He}$  production rates is bulk porosity of the crystalline basement largely controlled by fracture density.  $\text{H}_2$  production rates scale with porosity as more water is available for radiolysis, but  $\text{He}$  production rates are unaffected. The availability of water in proximity to radioelements in rocks may therefore be the limiting factor for  $\text{H}_2$  production in tight rocks. Bulk porosity estimates are between 0.1 and 2% globally for crystalline basement (Sherwood Lollar et al., 2014), but are based on relatively few empirical studies (e.g. Stober and Bucher, 2007 and references therein). The relative differences in basement architecture expressed as porosity present a key variable in these highly heterogeneous and isolated hydrogeological systems. In the following sections, the role of porosity as an important parameter controlling the crustal  $\text{He}$ ,  $\text{N}_2$ ,  $\text{CH}_4$  and  $\text{H}_2$  budget is explored.

#### 3.4. The production of $\text{H}_2$ , $\text{He}$ and $\text{N}_2$ in the subsurface

Radiolytic  $\text{H}_2$  is naturally produced within the subsurface by ionising radiation emitted as  $\alpha$ ,  $\beta$  and  $\gamma$  particles as part of the U, Th and K decay chains splitting the water molecule to produce  $\text{H}_2$  and short-lived oxidized radicals (Lin et al., 2005a, 2005b). The production of  $\text{H}_2$  is directly linked to  $\text{He}$  through the rate of  $\alpha$  particle generation. The production ratio of these two elements by radiolysis is correlated and can be assumed to be constant over time (due to long radioelement half-lives). The sites from the Witwatersrand basin discussed in this study are an ideal case study location for radiolysis because ultramafic minerals (source of water-rock reaction produced  $\text{H}_2$ ) are absent in the sampled units, primarily composed of quartzites, banded ironstones, mudstones, conglomerates (Witwatersrand Supergroup) (Robb and Meyer, 1995), overlaid by the Ventersdorp andesitic extrusive volcano-sedimentary sequence that has undergone medium grade metamorphism (Coward et al., 1995). The thermodynamic potential for  $\text{H}_2$  generation from sparse ultramafic intrusions is orders of magnitude lower than the observed concentrations and can be considered negligible (Lin et al., 2005b).

$\text{N}_2$  has multiple sources and sinks in the subsurface (thermal decomposition, microbial, radiolytic) and quantifying the link to  $\text{H}_2/\text{He}$  production is challenging. The radiolytic source presents an intriguing possibility for a direct link to  $\text{He}$  with existing evidence for multiple relevant reaction pathways. In the presence of oxygen, these include irradiation through dissociation of  $\text{N}_2\text{O}$  and reactions between N and O radicals (Spinks and Woods, 1990). In anoxic conditions that are more applicable to the fracture fluid setting,  $\text{N}_2\text{O}$  has been shown to scavenge hydrated electrons to form  $\text{N}_2\text{O}^-$  radicals that spontaneously decompose to form  $\text{N}_2$  (Eq. 1) (LaVerne and Pimblott, 1993; Nakken and Pihl, 1965). The kinetic rates of this reaction increase at alkaline pH conditions (Nakken and Pihl, 1965) which are observed in fracture fluid environments (Onstott et al., 2006). The electrons and hydrons required for the reaction are by-products of  $\text{H}_2\text{O}$  radiolysis and could in theory provide a framework for coupled radiolytic  $\text{H}_2$  and  $\text{N}_2$  production. Radicals

liberated during radiolysis can also oxidise the N species in solution to supply N<sub>2</sub>O. Irradiation experiments indicate NH<sub>3</sub> oxidation to NO<sub>3</sub><sup>-</sup> (Silver et al., 2012), formation of NH<sub>2</sub>O<sub>2</sub> radicals (Pagsberg, 1972), and further evidence for reactions between N radicals and O<sub>2</sub> to form NO<sub>2</sub><sup>-</sup> (Dwibedy et al., 1996).



While multiple lines of evidence exist for the theoretical basis of radiolytic N<sub>2</sub> production pathways, further studies at relevant thermodynamic conditions and gas/water volumes are required to confirm the full chain of radiolysis-induced reactions, their kinetic rates and the relative contribution to the overall N cycle.

### 3.5. H<sub>2</sub>, He and N<sub>2</sub> production rates

Theoretical He and H<sub>2</sub> production rates can be predicted for given radioelement concentrations using Eqs. (2)–(5). He is produced through  $\alpha$  decay of U and Th and expressed in molecules kg<sup>-1</sup> s<sup>-1</sup> (Eq. (2)) (Ballentine and Burnard, 2002). Y<sub>H2</sub> represents the total H<sub>2</sub> production rate (molecules kg<sup>-1</sup> s<sup>-1</sup>) (Eq. (2)) calculated based on methods by (Blair et al., 2007; Lin et al., 2005b); and equal to the sum of radiation doses (E<sub>Net,i</sub>) emitted through  $\alpha$ ,  $\beta$  and  $\gamma$  decay (particle denoted as i) multiplied by the radiolytic H<sub>2</sub> yields per unit of energy produced in water by radiolysis (G) in molecules/MeV (after Lin et al., 2005b). The radiation doses for a given type of radiation (Eq. 3) depend on radioelement concentration in ppm (X), decay energy (E) in Gy/ka (Adamiec and Aitken, 1998) converted to eV kg<sup>-1</sup> s<sup>-1</sup>, pore water to rock weight ratio (W), and the relative stopping power ratio (S) which indicates the ability of water to stop radiation relative to the rock (Hofmann, 1992). The weight ratio W (Eq. 5) depends on the relative densities ( $\rho$ ) in g/cm<sup>3</sup> of water and rock (denoted w, r) and porosity ( $\phi$ ), which is the main variable in the presented model. U, Th and K concentrations are of average upper continental crust (2.8 ppm, 10.7 ppm and 3.1 wt%, respectively (Rudnick and Fountain, 1995)). The parameters that are kept constant present a source of uncertainty (e.g. G values derived from laboratory experiments), however they are not expected to vary between different sampling sites.

(2)

$$Y_{H2} = \sum E_{Net,i} \times G_i \quad (3)$$

$$E_{Net,i} = E_{\alpha i} \times X \times W \times S_i / (1 + W \times S_i) \quad (4)$$

$$W = \frac{\phi \times \rho_w}{\rho_r \times (1 - \phi)} \quad (5)$$

### 3.6. Bayesian modelling of porosity influence to volatile mass balance

The control of porosity on the measured mass balance of observed volatiles (He, CH<sub>4</sub>, N<sub>2</sub>) can be tested using a Bayesian modelling framework. The advantage of the Bayesian method in this case is the possibility to use a priori knowledge about the plausible porosity ranges in the crystalline basement and therefore exclude unrealistic parameter values. This information can be formally included into the model as a prior probability distribution (referred to as ‘prior’) based on established knowledge about the system before the data is observed. Prior knowledge of the porosity parameter is combined with likelihood of the data given the model to obtain posterior probabilities for the hypothesis given the observed data.

The model considers a single variable (porosity) neglecting other gas sources and sinks (primarily non-methanogenic H<sub>2</sub> utilisation and gas loss through diffusion) and therefore represents the maximum effect porosity might have in the system. Negligible diffusive gas loss out of the system is supported by long residence times reported by previous studies

(Heard et al., 2018; Lippmann-Pipke et al., 2011; Lippmann et al., 2003). Radioelement concentrations are those of average upper crust (Rudnick and Fountain, 1995). Two alternative scenarios relevant to the local geological setting were tested and rejected: 1) Extreme localised U enrichment based on observed values in reefs within Witwatersrand Basin in the order of 500–2500 ppm (Pienaar et al., 2015) 2) Variable U/Th contents in the order of 50–80% from average crustal values as reported from individual core sample studies in the Witwatersrand (Lin et al., 2005b). Both of these scenarios result in enrichment in both H<sub>2</sub> and He and therefore cannot account for the low H<sub>2</sub>/He ratios (discussed further in the results section).

The Bayesian approach makes statistical conclusions about parameters ( $\theta$ ) based on the observed data (y) in terms of probability statements. All unknown quantities are treated as random variables that are assigned a prior probability distribution p( $\theta$ ) based on the existing information about the system. The observed data is assigned a joint probability distribution p(y| $\theta$ ) through a likelihood function, which describes the causal relationship between model parameters and data. In order to make inferences about model parameters, we construct posterior distribution p( $\theta$ |y), which is a joint distribution of all model parameters that are conditional on the observed data, and is constructed following the Bayes’ rule (Gelman et al., 2013):

$$p(\theta|y) \propto p(y|\theta)p(\theta) \quad (6)$$

In this model, He concentrations are the observed data y and porosity is the unknown parameter  $\theta$ . The dependency of y on  $\theta$  is described through a likelihood function. The final He concentrations in percent mole are expressed as He production rate (Eq. 2) normalised to the total production rate of all gases in the system ( $M_{t[b]}$ ) in mol/kg s<sup>-1</sup> (Eq. 6). N<sub>A</sub> is the Avogadro number, b denotes borehole.

$${}^4He_{mod[b]} = {}^4He_{prod} \times \frac{100 N_A}{M_{t[b]}} \quad (7)$$

$$M_{t[b]} = ({}^4He + CH_{4[b]} + N_{2,prod[b]}) \times N_A \quad (8)$$

To calculate  $M_{t[b]}$ , CH<sub>4</sub> and N<sub>2</sub> production rates have to be defined. Based on the isotopic and compositional data in Fig. 5, the samples in the dataset are dominantly microbial CH<sub>4</sub> produced by hydrogen utilisation. CH<sub>4</sub> production rate is calculated by multiplying H<sub>2</sub> production rate Y<sub>H2</sub> by a conversion factor Z (Eq. 9) which is a constant of 0.25, based on the stoichiometric 4:1 ratio between H<sub>2</sub> and CH<sub>4</sub>. Y and CH<sub>4</sub> values are modelled for individual boreholes, while the parameter Z is constant. N<sub>2</sub> production rate, as discussed previously, is the most challenging to constrain due to multiple sources and the total budget might consist of large volumes released episodically (thermal events) as well as continuous low temperature devolatilisation, radiolytic and microbial input. As previously discussed, the abiotic sources strongly depend on the NH<sub>4</sub> content of the host rock, and therefore are expected to vary across different sampling locations. The scenario tested in this model uses the observed N<sub>2</sub>/He in individual boreholes to relate N<sub>2</sub> and He production (Eq. 10). This approach represents an ‘apparent’ N<sub>2</sub> production ratio and encompasses both the possible N<sub>2</sub>/He link through radiolysis as well as the episodic release during thermal events, where He degassing would also be expected.

$$CH_{4[b]} = Y_{[b]} \times Z \quad (9)$$

$$N_{2[b]} = \quad (10)$$

By combining Eqs. 2–10, the final He concentrations in boreholes can be expressed as a function of porosity (Eq. 7), taking into account the associated radiolytic production of H<sub>2</sub> (and subsequent conversion to microbial CH<sub>4</sub>) and N<sub>2</sub>. The model samples parameters from prior distributions to achieve the best fit to the measured He values. The estimated model CH<sub>4</sub> concentrations can then be compared to the observed ones (not seen by the algorithm) to evaluate how accurately the model is

describing the real system. The hierarchical model structure allows to pool parameters between different samples, as well as individually fit for each borehole. He concentrations were modelled as a normal distribution with means  $\mu = [\mu_{b1} \dots \mu_B]$  and a half-normal distribution for the standard deviation hyper-prior. For the  $\varphi$  parameter (Eq. 5) an informative prior ( $N \sim (1,1)$ ) was used, where  $N$  is a normal distribution, numbers in brackets are mean and standard deviation, respectively), based on the existing empirical and modelling data constrains of porosity in crystalline basement of  $1 \pm 0.45\%$  (Sherwood Lollar et al., 2014 and references therein). Models were run using a Python package PyMC3 (Salvatier et al., 2016) for 10,000 iterations with NUTS (No-U-Turn Sampling) (Hoffman and Gelman, 2014) using two independent Markov chains. Each chain simultaneously performs 2000 burn-in steps which are discarded. Model posterior traces and posterior predictive checks were carried out to ensure model convergence, R-hat values were equal to 1 indicating convergence based on Gelman-Rubin statistics (Gelman et al., 2014).

### 3.7. Model results

The estimated posterior means for He concentrations are in agreement with the observed data points (RMSE = 0.9). Fig. 6a shows the posterior predictions within 95% highest density interval for He concentrations compared to the observed values. This result is consistent with porosity means for individual boreholes ranging between 0.3 and 2.2%, with a mean value of  $1.2 \pm 0.6\%$  ( $1\sigma$ ) (Fig. 6b). The predicted  $H_2/He$  ratios range between 21 and 166 (Table 1). The observed data is consistent with the hypothesis of in-situ fluid generation through radioelement decay and subsequent microbial utilisation, within a closed system.

Posterior predictions of  $CH_4$  concentrations based on  $H_2$  production rate and total conversion to  $CH_4$  are also in good agreement with the observed  $CH_4$  concentrations (Fig. 6c). The model underestimates the mean  $CH_4$  contents by 7% on average. FL1 is an exception where the model fit is poor due to low He contents (factor of 70 lower than the median sample), likely related to secondary He loss from the system. This leads to model underestimation of  $H_2$  and subsequent  $CH_4$  concentrations. FL1, SQ and EX1 (lowest He concentrations) are sensitive to the porosity prior and are also compatible with higher porosities (31%, 6.1% and 4.5% respectively) when an uninformative prior is chosen. In the case of FL1, this scenario can be discounted as not plausible in a crystalline basement setting, while SQ and EX1 could either represent outlier porosity cases, or indicate that other sources and sinks not represented by this model are significant. FL1 and SQ represent the lowest ( $3 \times 10^5$ – $4 \times 10^5$  L/day in the observation period) and the most variable flow rates in the sample set indicating low hydraulic conductivity, however the opposite would be expected if the low He concentrations in these samples were due to dilution by large gas volumes as a consequence of high porosity. It is therefore most likely that diffusive He loss occurred in FL1 and SQ. In contrast, the flow rate is among the highest ( $6 \times 10^6$  L/day) and sustained through the observation period in EX1, compatible with high porosity.

A simplified version of the model is also considered where  $N_2$  production, which presents the highest degree of uncertainty in terms of sources, is excluded. He,  $H_2$ ,  $CH_4$  are modelled according to Eqs. 3–5 and 8 using the measured  $CH_4/He$  ratios as the observed data and a flat prior for porosity. The porosity values here represent a simple best-fit scenario, and are in agreement with the original model in Fig. 6 and with high porosity estimates for the three samples discussed above (Sup. Fig. 1).

### 3.8. Potential radiolytic cycling of nitrogen

The model results show an intriguing relationship between  $N_2$  and  $H_2$  in the fluids (consistent ratio) in contrast to the variable porosity-dependent  $H_2/He$  ratio (Fig. 7a). Consistent  $N_2/H_2$  ratio raises the

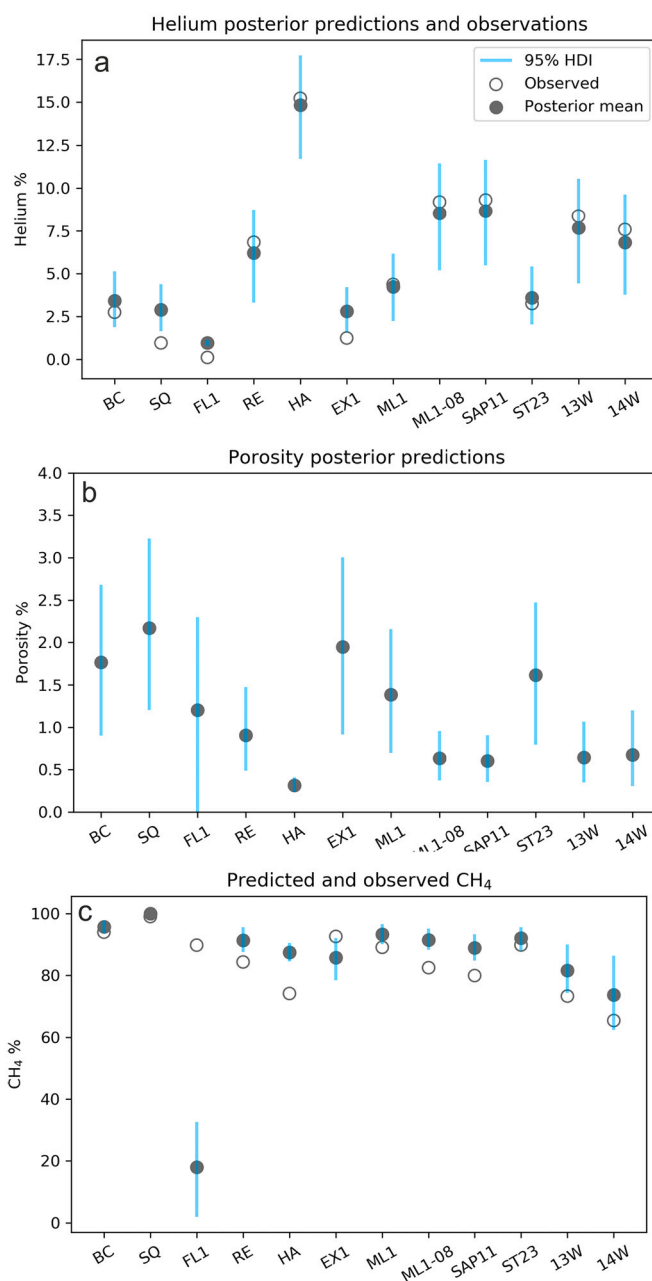


**Fig. 6.** a) Helium posterior predictions (the distribution of possible unobserved values given the observed helium values) for individual boreholes compared with the observed data. Blue line shows the 95% highest density interval. b) Posterior means for the porosity parameter. c)  $CH_4$  posterior predictions based on full  $H_2$  conversion to methane, using a 4:1 ratio where 4  $H_2$  molecules produce 1  $CH_4$  molecule. (For interpretation of the references to colour in this figure legend, the reader is referred to the web version of this article.)

possibility of a co-genetic link between radiolytic  $H_2$  and  $N_2$  and could suggest that radiolytic production might play a role in the nitrogen cycle at these sites. Indeed, previous work, (e.g. Silver et al., 2012) revealed how radiolysis can result in  $NO_3^-$  formation in these types of fluid. The consistency of the  $N_2$  and  $H_2$  model values in this study may suggest that a similar process acting on N-bearing compounds in the water phase could also directly produce  $N_2$ , or indirectly through the generation of substrates for microbial activity such as  $NO_3^-$ ,  $N_2O$  or  $NO$  (Sheik et al., 2021). Using the limited available experimental data, we use the relationship between  $NH_3$  conversion rates to  $NO_3^-$  and required radioactive dosage rates (Silver et al., 2012) to model  $NH_3$  concentrations



**Table 1**

Model posterior predictions. Last two columns show borehole depth and expected depth of the system based on the modelled porosity values.

Borehole	Porosity %	Porosity sd	He %	He sd	CH <sub>4</sub> %	CH <sub>4</sub> sd	H <sub>2</sub> /He	H <sub>2</sub> /He sd	N <sub>2</sub> /H <sub>2</sub>	N <sub>2</sub> /H <sub>2</sub> sd	Borehole depth (m)	Expected depth (m)*
BC	1.8	0.5	3.4	0.9	95.7	1.2	116	45	0.010	0.004	1092	na
SQ	2.2	0.6	2.9	0.8	100.0	3.0	143	54	0	0	1750	na
FL1	1.2	0.7	1.0	0.1	18.0	8.6	79	46	1.070	0.621	1288	1380
RE	0.9	0.3	6.2	1.4	91.4	2.1	60	24	0.022	0.009	514	2761
HA	0.3	0.1	14.8	1.6	87.5	1.6	21	4	0.034	0.007	–	8035
EX1	1.9	0.6	2.8	0.8	85.7	4.1	127	52	0.039	0.016	–	na
ML1	1.4	0.4	4.3	1.1	93.3	1.8	91	36	0.016	0.007	1237	641
ML1–08	0.6	0.2	8.5	1.6	91.4	1.8	42	15	0.022	0.008	1237	4708
SAP11	0.6	0.2	8.6	1.6	88.9	2.2	40	14	0.029	0.010	–	4708
ST23	1.6	0.5	3.6	1.0	92.0	2.2	106	42	0.020	0.008	580	310
13 W	0.6	0.2	7.7	1.6	81.7	4.1	42	18	0.052	0.021	–	4708
14 W	0.7	0.3	6.8	1.5	73.8	6.4	44	21	0.080	0.038	–	3968

\* Based on [Bethke \(1985\)](#) depth-porosity model using the modelled porosity values. Note that larger than 1.6% porosity is outside the model fit (na – not applicable).

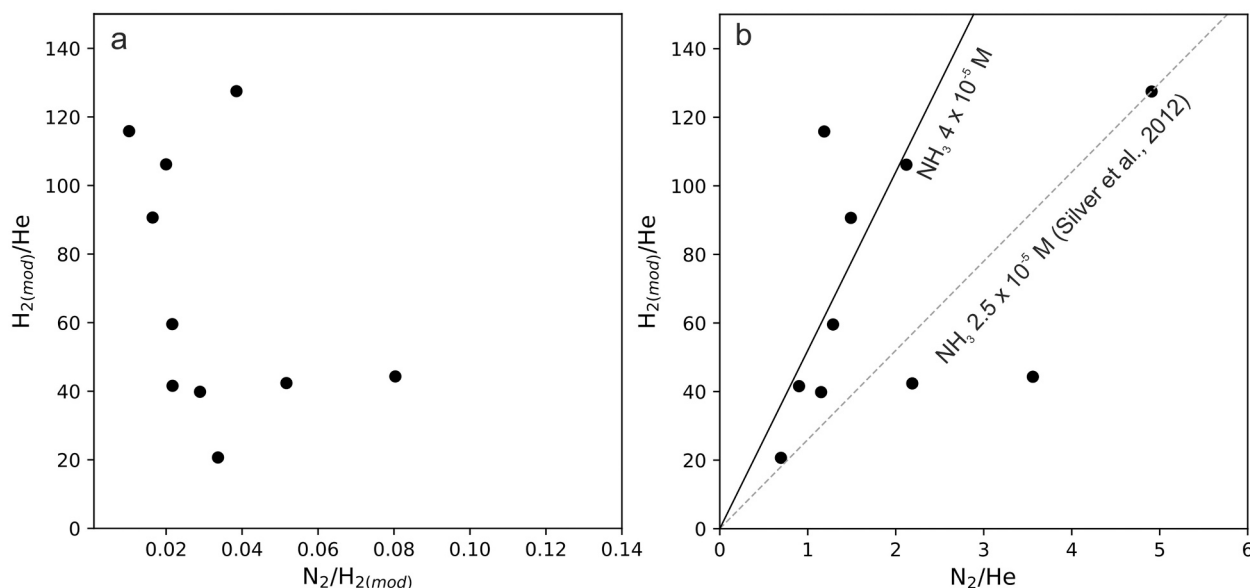


**Fig. 7.** a) H<sub>2</sub>/He vs N<sub>2</sub>/H<sub>2</sub> plot (model results). N<sub>2</sub>/H<sub>2</sub> ratios are consistent while H<sub>2</sub>/He ratios vary, suggesting that N<sub>2</sub> and H<sub>2</sub> production is linked. b) H<sub>2</sub>/He vs N<sub>2</sub>/He plot showing a strong non-parametric positive correlation between N<sub>2</sub> and H<sub>2</sub> (Spearman's rho = 0.6, p = 0.05). Dashed line shows the dependency between radiolytic H<sub>2</sub> production and NO<sub>3</sub><sup>−</sup> production using experimental data in [Silver et al. \(2012\)](#), assuming that all NO<sub>3</sub><sup>−</sup> subsequently is converted to N<sub>2</sub> through either abiotic or biological processes, and using NH<sub>3</sub> concentrations in their experiment. Solid black line shows the NH<sub>3</sub> concentrations required for a best fit line to the observed data.

needed to explain the N<sub>2</sub> contents, assuming that NO<sub>3</sub><sup>−</sup> is fully converted to N<sub>2</sub> either through further radiolytic or microbial reactions. The required NH<sub>3</sub> contents (solid line, [Fig. 8b](#)) are similar to those that have been measured in the pore fluids of Witwatersrand Basin core ([Silver et al., 2012](#)). Although the potential role of radiolytic production of N<sub>2</sub> is postulated here, this study highlights how additional work is needed to fully evaluate all possible pathways of production and processing of nitrogen in the deep subsurface.

## 4. Implications

### 4.1. Abiotic controls on gas generation within a closed system

The dataset is consistent with a hydrogeologically closed system where the He/H<sub>2</sub>/CH<sub>4</sub> mass balance can be accounted for by radiogenic decay products and hydrogenotrophic methanogenesis, with a potential significant radiolytic control on N<sub>2</sub> among other sources (summarised in [Fig. 9](#)). The model demonstrates the maximum effect porosity may have on abiotic production of crustal volatiles in fractured Precambrian basement. Alternative processes cannot be discounted and may result in

similar mass balance distributions, most notably H<sub>2</sub> loss to other microbial metabolisms, in particular sulfate-reducing bacteria observed in many fracture fluid environments ([Kieft et al., 2005](#); [Lau et al., 2016](#); [Lin et al., 2006](#); [Chivian et al., 2008](#)). The relative uptake of H<sub>2</sub> for sulfate reduction in this system is unknown, however the end-product of this metabolic pathway (H<sub>2</sub>O) ([Li et al., 2016](#)) replenishes the total water budget that can be further ionised to create more H<sub>2</sub>. If the availability of water (as a function of porosity) is the limiting factor for H<sub>2</sub> and subsequent microbial CH<sub>4</sub> generation, the presence of sulfate reducing bacteria should not have a significant impact on the final gas mass balance because the water is recycled through their metabolism.

Given the highly heterogeneous architecture of fracture networks, slow water flow rates, long residence times characteristic of these environments as well as variation in lithologies (Witwatersrand Supergroup, Ventersdorp, Karoo) and depths (Table S4), the proposed porosity control scenario is highly plausible. The predicted values represent bulk porosity over the volume of rock in which the sampled fluids are produced, which might vary between the sampling sites, however all volumes are substantially large to produce continuous gas flow over the period of 14 months ([Fig. 3](#)). Using the depth-porosity

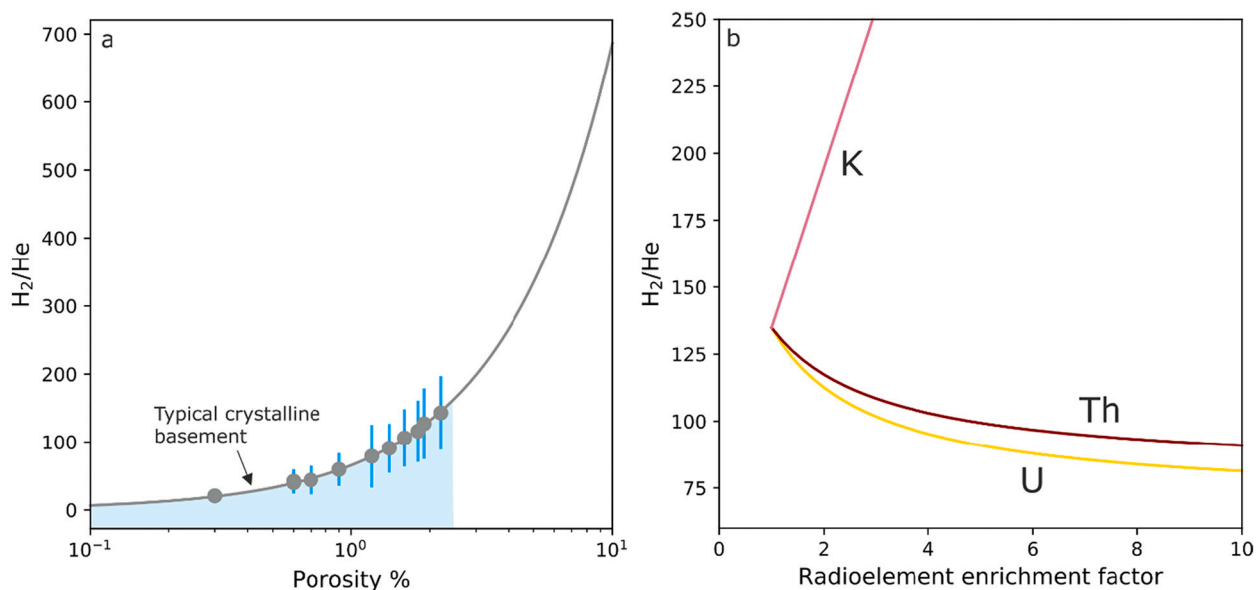


**Fig. 8.** a)  $H_2/He$  ratio as a function of porosity which controls the amounts of water available for radiolysis. Typical crystalline basement porosity values yield  $H_2/He$  ratios between 6.5 and 132. Modelled  $H_2/He$  ratios for the borehole samples are shown with  $1\sigma$  error. b)  $H_2/He$  ratio as a function of radioelement concentration expressed as an enrichment factor from average upper crust values assuming 1% porosity. Variation of radioelements cannot account for  $H_2/He$  ratios below 80.

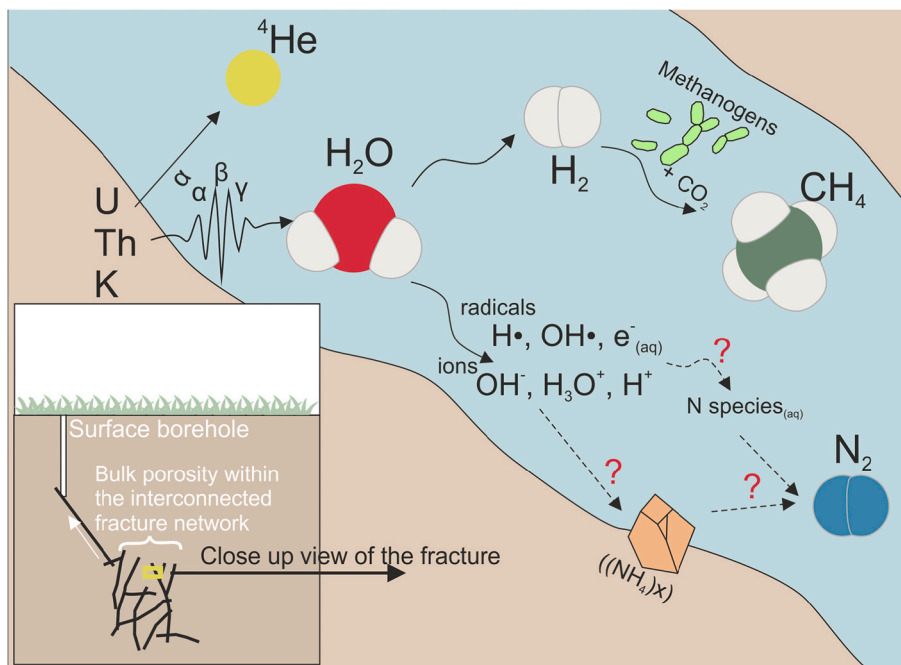


**Fig. 9.** Schematic cartoon depicting processes contributing to the production of gases sampled at surface boreholes. The image on the left shows the borehole intercepting an interconnected fracture network and fluids are transported to the surface. Radioelement (U, Th, K) decay produces  $^4He$  (directly) and  $H_2$  (through radiolysis).  $H_2$  is consumed by methanogens producing microbial  $CH_4$ . Water molecule radiolysis also produces highly reactive radicals and ions which react with fracture minerals (Li et al., 2016; Sherwood Lollar et al., 2021). These reactions (either with  $NH_4$  contained within phyllosilicates or dissolved N species (Silver et al., 2012)) may potentially form  $N_2$ , however more work is needed to investigate this pathway.

model (Bethke, 1985) applied in Sherwood Lollar et al. (2014), the expected porosity values at the bottom of the sampled boreholes (where depth is known) should range between 1.1 and 1.4%. The model-predicted porosity values are lower in many of the boreholes (0.3–2.2%, Table 1), suggesting that  $H_2$  generation might be occurring within fracture networks at lower depths, intersected by a fault or fracture network (potentially produced during drilling) that transports the fluids to the surface (Fig. 9). The modelled porosity values are consistent with depths between 310 and 8035 m (Table 1, note that values with higher than 1.6% porosity are outside of the model fit).

The variation of porosity as a single parameter within the range of typical crustal values (0.1–2.1%) using the average upper crust radioelement concentrations produces  $H_2/He$  range of 6.5–138 (Fig. 8a).

Theoretically, if only in-situ He and  $H_2$  production is considered, and all  $H_2$  is subsequently converted to  $CH_4$ , porosity can account for resulting He concentrations between 3 and 62%. This effect is much higher than from other important abiotic parameters such as local enrichment of U and Th that may lead to lower  $H_2/He$  ratios (but still  $>80$ ), while enrichment in K sharply increases the ratio because the  $\alpha$  particle is not a part of the K decay chain (Fig. 8b).

#### 4.2. Abiotic controls on subsurface habitability

Radiolysis may play a key role in controlling the subsurface habitability of the Earth and other planets, with increasing body of evidence showing not only production of  $H_2$ , but also electron donors (Li et al.,

2016) and organic acids (Sherwood Lollar et al., 2021). The extent of all viable radiolytic reactions under relevant thermodynamic conditions require future studies, however these early results demonstrate the potential for closed-system radiolytically-driven nutrient supply for microbial ecosystems. The hydrogeological environment described in this study is an example of a such a cycle at the basis of an organic C cycle dominated by methanogens.

Methanogenesis is typically limited by water salinity when the bioenergetic cost of  $H_2$  utilisation approaches the energy available from the metabolic pathway. Such environments are expected to be at least  $>1.9$  M in ionic strength (Telling et al., 2018), providing a bracket to the range of extreme environmental conditions where microbial ecosystems are unable to utilise this molecule above its slow synthesis rates. The sampled system is likely below this threshold (in line with observations in South African mine samples reporting relatively low salinities between 188 and 4473 ppm (Magnabosco et al., 2014) and represents an environment where  $H_2$  source has been exhausted and the microbial community is dormant. This means that porosity and therefore the availability of water for radiolysis might be one of the limiting factors for certain types of life, such as hydrogenotrophic methanogens in the deep subsurface. Certainly, the variable total methane contents in different sampling locations (inferred from flow rate data and the degree of He dilution) demonstrate how the basement architecture is a significant limiting factor in the productivity of chemosynthetic microbial communities.

#### 4.3. Closed system high-He and $CH_4$ environments

From the perspective of He exploration in crystalline basement environments, lithologies with the lowest porosity are favourable for limited  $H_2$  and therefore  $CH_4$  production that would otherwise dilute He. This is demonstrated by sample HA which has the highest observed He contents (15%) and the lowest predicted porosity value of  $0.3 \pm 0.1\%$ . Typically, high He systems require long periods of quiescence for He accumulation, followed by fluid mobilisation, typically by another migrating gas phase, followed by transport over long distances and high degree of interaction with groundwater (e.g. Ballentine and Sherwood Lollar, 2002; Danabalan, 2017; Gilfillan et al., 2008). The Witwatersrand Basin presents an alternative closed system model, where the hydrogeological systems are isolated, gas generation occurs in-situ driven by radioelement decay, and no external input is required. The proposed gas generation mechanism is also novel in the context of our understanding of  $CH_4$  in the subsurface in potentially commercial volumes. Contrary to conventional hydrocarbon systems, the system described here is not associated with the presence organic source rock, and offers an alternative interpretation to previously proposed hydrocarbon generation models in the Karoo Basin (Eymold et al., 2018). The prevalence of methanogens in this system is however controlled by the availability of C-bearing substrate, which may be available in the form of carbonate minerals (Sohlberg et al., 2015), organic matter in meta-sediments (Petsch et al., 2001) or indeed produced through radiolysis (Sherwood Lollar et al., 2021).

#### 4.4. Implications for $H_2$ exploration

Anthropogenic activity through borehole drilling and introduction of oxygen-rich meteoric water into the system (e.g. Ebigbo et al., 2013) may catalyse sudden microbial blooms, if any  $H_2$  is present in the system prior to exploration. In this scenario, aerobic oxidation ( $2H_2 + O_2 \rightarrow 2H_2O$ ) would be the dominant and energetically more efficient  $H_2$  utilisation in the presence of oxygen (Telling et al., 2018).  $CH_4$  generation through meteoric water introduction is therefore unlikely, however any residual  $H_2$  in the system could be converted to  $H_2O$  during fluid ascent. The implications of this discussion to commercial  $H_2$  exploration are two-fold. In this particular system, the bulk of hydrogenotrophic microbial  $H_2$  utilisation is operating over geological timescales rather than

rapidly due to fluid mixing after anthropogenic activity (drilling), therefore  $H_2$  discoveries in these particular localities are unlikely. However, the closed system model implies strictly in-situ  $H_2$  utilisation without evidence for external flux from depth. It is therefore likely that  $H_2$  produced at lower depths is not lost to overlying formations through diffusion or fracture-induced mixing, and may be conserved in fracture systems where methanogens are limited by hypersalinity (e.g. Sherwood Lollar et al., 2006).

## 5. Conclusions

Gas samples from exploration boreholes in Witwatersrand Basin ( $n = 12$ ) are dominated by microbial hydrocarbons (primarily  $CH_4$ ), concurring with high levels of  $N_2$  (3–27%) and He (0.1–15%). Despite high He concentrations, radiolytic  $H_2$  (linked to production of He through U/Th decay) is below detection limit. Using a Bayesian modelling approach, we demonstrate that the observed gas mass balance is consistent with in-situ fluid generation primarily through radioelement decay-driven processes, and subsequent conversion of radiolytic  $H_2$  to  $CH_4$  through hydrogenotrophic methanogenesis. The range of observed gas concentrations is consistent with a variation in in-situ porosity between 0.3 and 2.2%. The Witwatersrand basin presents an intriguing case of a closed-system He-rich natural gas, which is generated without an organic-rich source rock and does not require fluid mobilisation and migration over long distances. The activity of hydrogenotrophic microbial communities is the limiting factor for commercial  $H_2$  discoveries, which are more probable in hypersaline systems which inhibit the microbial metabolisms. The clear differences in porosity values between boreholes located in  $80\text{km}^2$  area suggest that these systems are localised, heterogeneous and not laterally interconnected. This study demonstrates how abiotic parameters such as porosity may be key in supporting or limiting the occurrence and productivity of chemosynthetic microbial communities, relevant to the search of life on other planets.

## Declaration of Competing Interest

The authors declare that they have no known competing financial interests or personal relationships that could have appeared to influence the work reported in this paper.

## Acknowledgements

BSL and CJB are CIFAR Fellows in the Earth-4D Subsurface Science Exploration Program. This research is based on work supported by the CIFAR Program in Earth 4D: Subsurface Science and Exploration through a catalyst award and the Africa Oxford Initiative grant. This study was financially supported by the Natural Sciences and Engineering Research Council of Canada (NSERC) Discovery and Accelerator grants. EH was supported by Technology Innovation Agency in South Africa. We thank D.J. Opperman and A. P. Bester for assistance in sample collection, mine operators for allowing to access the sampling sites, and K. Bayliss for insightful comments.

## Appendix A. Supplementary data

Supplementary data to this article can be found online at <https://doi.org/10.1016/j.chemgeo.2022.120788>.

## References

- Adamiec, G., Aitken, M.J., 1998. Dose-rate conversion factors: update. *Ancient TL* 16, 37–50.
- Ballentine, C.J., Burnard, P.G., 2002. Production, release and transport of noble gases in the continental crust. *Rev. Mineral. Geochem.* 47, 481–538. <https://doi.org/10.2138/rmg.2002.47.12>.

- Ballentine, C.J., Sherwood Lollar, B., 2002. Regional groundwater focusing of nitrogen and noble gases into the Hugoton-Panhandle giant gas field, USA. *Geochim. Cosmochim. Acta* 66, 2483–2497. [https://doi.org/10.1016/S0016-7037\(02\)00850-5](https://doi.org/10.1016/S0016-7037(02)00850-5).
- Bare, S.R., Lilly, M., Chermak, J., Eggert, R., Halperin, W., Hannahs, S., Hayes, S., Hendrich, M., Hurd, A., Osofsky, M., 2016. Responding to the US Research Community's Liquid Helium Crisis. American Physical Society; Materials Research Society. American Chemical Society. <https://doi.org/10.7936/K7571B6D>.
- Bethke, C.M., 1985. A numerical model of compaction-driven groundwater flow and heat transfer and its application to the paleohydrology of intracratonic sedimentary basins. *J. Geophys. Res. Solid Earth* 90, 6817–6828.
- Blair, C.C., D'Hondt, S., Spivack, A.J., Kingsley, R.H., 2007. Radiolytic hydrogen and microbial respiration in subsurface sediments. *Astrobiology* 7, 951–970.
- Borgonie, G., Magnabosco, C., García-Moyano, A., Linage-Alvarez, B., Ojo, A.O., Freese, L.B., Van Jaarsveld, C., Van Rooyen, C., Kuloyo, O., Cason, E.D., Vermeulen, J., Pienaar, C., Van Heerden, E., Sherwood Lollar, B., Onstott, T.C., Mundle, S.O.C., 2019. New ecosystems in the deep subsurface follow the flow of water driven by geological activity. *Sci. Rep.* 9, 1–16. <https://doi.org/10.1038/s41598-019-39699-w>.
- Bowen, T.B., Marsh, J.S., Bowen, M.P., Eales, H.V., 1986. Volcanic rocks of the Witwatersrand triad, south Africa. I: Description, classification and geochemical stratigraphy. *Precambrian Res.* 31, 297–324. [https://doi.org/10.1016/0301-9268\(86\)90038-0](https://doi.org/10.1016/0301-9268(86)90038-0).
- Chivian, D., Brodie, E.L., Alm, E.J., Culley, D.E., Dehal, P.S., DeSantis, T.Z., Gihring, T.M., Lapidus, A., Lin, L.-H., Lowry, S.R., 2008. Environmental genomics reveals a single-species ecosystem deep within Earth. *Science* (80). 322, 275–278.
- Cornell, D.H., Meintjes, P.G., Van der Westhuizen, W.A., Kristoffersen, M., Frei, D., 2021. Dating detrital zircon from the gold-bearing Ventersdorp Contact Reef in the Ventersdorp Supergroup of South Africa. *Precambrian Res.* 357, 106131.
- Coveney, R.M., Goebel, E.D., Zeller, E.J., Dreschhoff, G.A.M., Angino, E.E., 1987. Serpentinization and the origin of hydrogen gas in Kansas. *Am. Assoc. Pet. Geol. Bull.* 71, 39–48.
- Coward, M.P., Spencer, R.M., Spencer, C.E., 1995. Development of the Witwatersrand Basin, South Africa. *Geol. Soc. London Spec. Publ.* 95, 243–269.
- D'Hondt, S., Spivack, A.J., Pockalny, R., Ferdelman, T.G., Fischer, J.P., Kallmeyer, J., Abrams, L.J., Smith, D.C., Graham, D., Hasiuk, F., 2009. Subseafloor sedimentary life in the South Pacific Gyre. *Proc. Natl. Acad. Sci.* 106, 11651–11656.
- D'Hondt, S., Pockalny, R., Fulfer, V.M., Spivack, A.J., 2019. Subseafloor life and its biogeochemical impacts. *Nat. Commun.* 10, 1–13. <https://doi.org/10.1038/s41467-019-11450-z>.
- Danabalan, D., 2017. Helium: Exploration Methodology for a Strategic Resource. PhD Thesis. University of Durham.
- Doane, T.A., 2017. The abiotic nitrogen cycle. *ACS Earth Sp. Chem.* 1, 411–421.
- Doerfert, S.N., Reichlen, M., Iyer, P., Wang, M., Ferry, J.G., 2009. *Methanobrevibacterium zinderi* sp. nov., a methylophilic methanogen isolated from a deep subsurface coal seam. *Int. J. Syst. Evol. Microbiol.* 59, 1064–1069.
- Dwibedy, P., Kishore, K., Dey, G.R., Moorthy, P.N., 1996. Nitrite formation in the radiolysis of aerated aqueous solutions of ammonia. *Radiat. Phys. Chem.* 48, 743–747. [https://doi.org/10.1016/S0969-806X\(96\)00037-0](https://doi.org/10.1016/S0969-806X(96)00037-0).
- Ebigbo, A., Golfier, F., Quintard, M., 2013. A coupled, pore-scale model for methanogenic microbial activity in underground hydrogen storage. *Adv. Water Resour.* 61, 74–85.
- Etiopie, G., Sherwood Lollar, B., 2013. Abiotic Methane on Earth. *Rev. Geophys.* 51, 276–299. <https://doi.org/10.1002/rog.20011>.
- Eymold, W.K., Swana, K., Moore, M.T., Whyte, C.J., Harkness, J.S., Talma, S., Murray, R., Moortgat, J.B., Miller, J., Vengosh, A., Darrah, T.H., 2018. Hydrocarbon-rich groundwater above shale-gas formations: a karoo basin case study. *Groundwater* 56, 204–224. <https://doi.org/10.1111/gwat.12637>.
- Frimmel, H.E., 2019. The Witwatersrand Basin and its gold deposits. In: *The Archaeology of the Kaapvaal Craton, Southern Africa*. Springer, pp. 255–275.
- Gelman, A., Carlin, J.B., Stern, H.S., Dunson, D.B., Vehtari, A., Rubin, D.B., 2013. *Bayesian Data Analysis*, 2<sup>nd</sup> Ed. CRC press.
- Gelman, A., Carlin, J.B., Stern, H.S., Rubin, D.B., 2014. *Bayesian Data Analysis*, Vol. 2. Taylor & Francis Milton Park.
- Gihring, T.M., Moser, D.P., Lin, L.-H., Davidson, M., Onstott, T.C., Morgan, L., Milleson, M., Kieft, T.L., Trimarco, E., Balkwill, D.L., 2006. The distribution of microbial taxa in the subsurface water of the Kalahari Shield, South Africa. *Geomicrobiol. J.* 23, 415–430.
- Gilfillan, S.M.V., Ballentine, C.J., Holland, G., Blagburn, D., Sherwood Lollar, B., Stevens, S., Schoell, M., Cassidy, M., 2008. The noble gas geochemistry of natural CO<sub>2</sub> gas reservoirs from the Colorado Plateau and Rocky Mountain provinces, USA. *Geochim. Cosmochim. Acta* 72, 1174–1198. <https://doi.org/10.1016/j.gca.2007.10.009>.
- Granger, J., Sigman, D.M., Lehmann, M.F., Tortell, P.D., 2008. Nitrogen and oxygen isotope fractionation during dissimilatory nitrate reduction by denitrifying bacteria. *Limnol. Oceanogr.* 53, 2533–2545. <https://doi.org/10.4319/lo.2008.53.6.2533>.
- Greene, S., Battye, N., Clark, I., Kotzer, T., Bottomley, D., 2008. Canadian Shield brine from the Con Mine, Yellowknife, NT, Canada: Noble gas evidence for an evaporated Palaeozoic seawater origin mixed with glacial meltwater and Holocene recharge. *Geochim. Cosmochim. Acta* 72, 4008–4019.
- Heard, A.W., Warr, O., Borgonie, G., Linage, B., Kuloyo, O., Fellowes, J.W., Magnabosco, C., Lau, M.C.Y., Erasmus, M., Cason, E.D., van Heerden, E., Kieft, T.L., Mabry, J.C., Onstott, T.C., Sherwood Lollar, B., Ballentine, C.J., 2018. South African crustal fracture fluids preserve paleometeoric water signatures for up to tens of millions of years. *Chem. Geol.* 493, 379–395. <https://doi.org/10.1016/j.chemgeo.2018.06.011>.
- Hoffman, M.D., Gelman, A., 2014. The No-U-Turn sampler: adaptively setting path lengths in Hamiltonian Monte Carlo. *J. Mach. Learn. Res.* 15, 1593–1623.
- Hofmann, B.A., 1992. Isolated reduction phenomena in red beds: A result of porewater radiolysis? In: *International Symposium on Water-Rock Interaction*, pp. 503–506.
- Holland, G., Sherwood Lollar, B., Li, L., Lacrampe-Couloume, G., Slater, G.F., Ballentine, C.J., 2013. Deep fracture fluids isolated in the crust since the Precambrian era. *Nature* 497, 357–360. <https://doi.org/10.1038/nature12127>.
- Hunt, J.M., 1996. *Petroleum Geochemistry and Geology*. WH Freeman Company, New York.
- Kamo, S.L., Reimold, W.U., Krogh, T.E., Colliston, W.P., 1996. A 2.023 Ga age for the Vredefort impact event and a first report of shock metamorphosed zircons in pseudotachylitic breccias and granophyre. *Earth Planet. Sci. Lett.* 144, 369–387.
- Kietäväinen, R., Purkamo, L., 2015. The origin, source, and cycling of methane in deep crystalline rock biosphere. *Front. Microbiol.* 6, 725.
- Kieft, T.L., McCuddy, S.M., Onstott, T.C., Davidson, M., Lin, L.H., Mislowski, B., Pratt, L., Boice, E., Lollar, B.S., Lippmann-Pipke, J., Pfiffner, S.M., Phelps, T.J., Gihring, T., Moser, D., van Heerden, A., 2005. Geochemically generated, energy-rich substrates and indigenous microorganisms in deep, ancient groundwater. *Geomicrobiol. J.* 22, 325–335. <https://doi.org/10.1080/01490450500184876>.
- Kietäväinen, R., Ahonen, L., Kukkonen, I.T., Niedermann, S., Wiersberg, T., 2014. Noble gas residence times of saline waters within crystalline bedrock, Outokumpu Deep Drill Hole, Finland. *Geochim. Cosmochim. Acta* 145, 159–174.
- Kietäväinen, R., Ahonen, L., Niinikoski, P., Nykänen, H., Kukkonen, I.T., 2017. Abiotic and biotic controls on methane formation down to 2.5 km depth within the Precambrian Fennoscandian Shield. *Geochim. Cosmochim. Acta* 202, 124–145.
- Kloppmann, W., Girard, J.P., Négrel, P., 2002. Exotic stable isotope compositions of saline waters and brines from the crystalline basement. *Chem. Geol.* 184, 49–70. [https://doi.org/10.1016/S0009-2541\(01\)00352-7](https://doi.org/10.1016/S0009-2541(01)00352-7).
- Knipe, R.J., 1997. Juxtaposition and seal diagrams to help analyze fault seals in hydrocarbon reservoirs. *Am. Assoc. Pet. Geol. Bull.* 81, 187–195.
- Kotelnikova, S., 2002. Microbial production and oxidation of methane in deep subsurface. *Earth-Sci. Rev.* 58, 367–395.
- Lau, M.C.Y., Kieft, T.L., Kuloyo, O., Linage-Alvarez, B., Van Heerden, E., Lindsay, M.R., Magnabosco, C., Wang, W., Wiggins, J.B., Guo, L., 2016. An oligotrophic deep-subsurface community dependent on syntrophy is dominated by sulfur-driven autotrophic denitrifiers. *Proc. Natl. Acad. Sci.* 113, E7927–E7936.
- LaVerne, J.A., Pimblott, S.M., 1993. Yields of hydroxyl radical and hydrated electron scavenging reactions in aqueous solutions of biological interest. *Radiat. Res.* 135, 16–23.
- Li, L., Cartigny, P., Ader, M., 2009. Kinetic nitrogen isotope fractionation associated with thermal decomposition of NH<sub>3</sub>: Experimental results and potential applications to trace the origin of N<sub>2</sub> in natural gas and hydrothermal systems. *Geochim. Cosmochim. Acta* 73, 6282–6297. <https://doi.org/10.1016/j.gca.2009.07.016>.
- Li, L., Li, K., Giunta, T., Warr, O., Labidi, J., Sherwood Lollar, B., 2021. N<sub>2</sub> in deep subsurface fracture fluids of the Canadian Shield: source and possible recycling processes. *Chem. Geol.* 585, 120571. <https://doi.org/10.1016/j.chemgeo.2021.120571>.
- Li, L., Sherwood Lollar, B., Li, H., Wortmann, U.G., Lacrampe-Couloume, G., 2012. Ammonium stability and nitrogen isotope fractionations for NH<sub>4</sub>–NH<sub>3</sub> (aq)–NH<sub>3</sub> (gas) systems at 20–70 °C and pH of 2–13: applications to habitability and nitrogen cycling in low-temperature hydrothermal systems. *Geochim. Cosmochim. Acta* 84, 280–296. <https://doi.org/10.1016/j.gca.2012.01.040>.
- Li, L., Wing, B.A., Bui, T.H., McDermott, J.M., Slater, G.F., Wei, S., Lacrampe-Couloume, G., Sherwood Lollar, B., 2016. Sulfur mass-independent fractionation in subsurface fracture waters indicates a long-standing sulfur cycle in Precambrian rocks. *Nat. Commun.* 7. <https://doi.org/10.1038/ncomms13252>.
- Lin, L.-H., Slater, G.F., Sherwood Lollar, B., Lacrampe-Couloume, G., Onstott, T.C., 2005a. The yield and isotopic composition of radiolytic H<sub>2</sub>, a potential energy source for the deep subsurface biosphere. *Geochim. Cosmochim. Acta* 69, 893–903. <https://doi.org/10.1016/j.gca.2004.07.032>.
- Lin, L., Hall, J., Lippmann-Pipke, J., Ward, J.A., Sherwood Lollar, B., DeFlaun, M., Rothmel, R., Moser, D., Gihring, T.M., Mislowski, B., Onstott, T.C., 2005b. Radiolytic H<sub>2</sub> in continental crust: Nuclear power for deep subsurface microbial communities. *Geochim. Geophys. Geosyst.* 6. <https://doi.org/10.1029/2004GC000907>.
- Lin, L.H., Wang, P.-L., Rumble, D., Lippmann-Pipke, J., Boice, E., Pratt, L.M., Lollar, B.S., Brodie, E.L., Hazen, T.C., Andersen, G.L., DeSantis, T.Z., Moser, D.P., Kershaw, D., Onstott, T.C., 2006. Long-Term Sustainability of a High-Energy, Low-Diversity Crustal Biome. *Science* (80). 314, 479–482. <https://doi.org/10.1126/science.1127376>.
- Lippmann, J., Stute, M., Torgersen, T., Moser, D.P., Hall, J.A., Lin, L., Borsik, M., Bellamy, R.E.S., Onstott, T.C., 2003. Dating ultra-deep mine waters with noble gases and <sup>36</sup>Cl, Witwatersrand Basin, South Africa. *Geochim. Cosmochim. Acta* 67, 4597–4619. [https://doi.org/10.1016/S0016-7037\(03\)00414-9](https://doi.org/10.1016/S0016-7037(03)00414-9).
- Lippmann-Pipke, J., Sherwood Lollar, B., Niedermann, S., Stronck, N.A., Naumann, R., van Heerden, E., Onstott, T.C., 2011. Neon identifies two billion year old fluid component in Kaapvaal Craton. *Chem. Geol.* 283, 287–296. <https://doi.org/10.1016/j.chemgeo.2011.01.028>.
- Lollar, G.S., Warr, O., Telling, J., Osburn, M.R., Sherwood Lollar, B., 2019. 'Follow the Water': hydrogeochemical constraints on microbial investigations 2.4 km below surface at the Kidd creek deep fluid and deep life observatory. *Geomicrobiol. J.* 36, 859–872. <https://doi.org/10.1080/01490451.2019.1641770>.
- Magnabosco, C., Tekere, M., Lau, M.C.Y., Linage, B., Kuloyo, O., Erasmus, M., Cason, E., van Heerden, E., Borgonie, G., Kieft, T.L., Olivier, J., Onstott, T.C., 2014. Comparisons of the composition and biogeographic distribution of the bacterial communities occupying South African thermal springs with those inhabiting deep



- subsurface fracture water. *Front. Microbiol.* 5 <https://doi.org/10.3389/fmicb.2014.00679>.
- Magnabosco, C., Lin, L.-H., Dong, H., Bomberg, M., Ghiorse, W., Stan-Lotter, H., Pedersen, K., Kieft, T.L., Van Heerden, E., Onstott, T.C., 2018. The biomass and biodiversity of the continental subsurface. *Nat. Geosci.* 11, 707–717.
- McCollom, T.M., Bach, W., 2009. Thermodynamic constraints on hydrogen generation during serpentinization of ultramafic rocks. *Geochim. Cosmochim. Acta* 73, 856–875.
- Mkhabela, M., Manzi, M., 2017. Detection of potential methane gas pathways in deep South African gold mines. *J. Geophys. Eng.* 14, 960–974. <https://doi.org/10.1088/1742-2140/aa6fc8>.
- Nakken, K.F., Pihl, A., 1965. On the ability of nitrous oxide to convert hydrated electrons into hydroxyl radical. *Radiat. Res.* 26, 519–526.
- Omar, G.I., Onstott, T.C., Hoek, J., 2003. The origin of deep subsurface microbial communities in the Witwatersrand basin, South Africa as deduced from apatite fission track analyses. *Geofluids* 3, 69–80. <https://doi.org/10.1046/j.1468-8123.2003.00050.x>.
- Onstott, T.C., Lin, L.H., Davidson, M., Mislowski, B., Borsik, M., Hall, J., Slater, G., Ward, J., Sherwoodlollar, B., Lippmann-Pipke, J., Boice, E., Pratt, L.M., Pfiffner, S., Moser, D., Gihring, T., Kieft, T.L., Phelps, T.J., Vanheerden, E., Litthaur, D., Deflaun, M., Rothmel, R., Wanger, G., Southam, G., 2006. The origin and age of biogeochemical trends in deep fracture water of the Witwatersrand basin, South Africa. *Geomicrobiol. J.* 23, 369–414. <https://doi.org/10.1080/01490450600875688>.
- Oremland, R.S., 1988. Biogeochemistry of methanogenic bacteria. *Biol. Anaerob. Microorg.* 641–705.
- Pagsberg, P.B., 1972. Investigation of the  $\text{NH}_2$  radical produced by pulse radiolysis of ammonia in aqueous solution. *Asp. Res. Riso* 5, 209.
- Petsch, S.T., Eglinton, T.I., Edwards, K.J., 2001. 14C-dead living biomass: evidence for microbial assimilation of ancient organic carbon during shale weathering. *Science* (80-. ) 292, 1127–1131.
- Pienaar, D., Guy, B.M., Hofmann, A., Viljoen, K.S., 2015. A geometallurgical characterization of the Vaal Reef A-facies at the Moab Khotsong mine, Klerksdorp Goldfield, South Africa. *South African J. Geol.* 118, 455–472.
- Pitkänen, P., Partamies, S., 2007. Origin and implications of dissolved gases in groundwater at Olkiluoto (POSIVA-07-04). Finland. Available in fulltext at. <http://www.posiva.fi/raportit/Posiva2007-04web.pdf>.
- Robb, L.J., Meyer, F.M., 1995. The Witwatersrand Basin, South Africa: Geological framework and mineralization processes, 10, pp. 67–94.
- Robb, L.J., Charlesworth, E.G., Drennan, G.R., Gibson, R.L., Tongu, E.L., 1997. Tectono-metamorphic setting and paragenetic sequence of Au-U mineralisation in the Archaean Witwatersrand Basin, South Africa. *Aust. J. Earth Sci.* 44, 353–371.
- Rudnick, R.L., Fountain, D.M., 1995. Nature and composition of the continental crust: a lower-crustal perspective. *Rev. Geophys.* 33, 267–309. <https://doi.org/10.1029/95rg01302>.
- Rufer, D., Waber, H.N., Gimmi, T., 2018. Identifying temporally and spatially changing boundary conditions at an aquifer – aquitard interface using helium in porewater. *Appl. Geochem.* 96, 62–77. <https://doi.org/10.1016/j.apgeochem.2018.05.022>.
- Salvatier, J., Wiecki, T.V., Fonnesbeck, C., 2016. Probabilistic programming in Python using PyMC3. *PeerJ. Comput. Sci.* 2, e55.
- Sauvage, J.F., Flinders, A., Spivack, A.J., Pockalny, R., Dunlea, A.G., Anderson, C.H., Smith, D.C., Murray, R.W., D'Hondt, S., 2021. The contribution of water radiolysis to marine sedimentary life. *Nat. Commun.* 12, 1297. <https://doi.org/10.1038/s41467-021-21218-z>.
- Schoell, M., 1988. Multiple origins of methane in the Earth. *Chem. Geol.* 71, 1–10. [https://doi.org/10.1016/0009-2541\(88\)90101-5](https://doi.org/10.1016/0009-2541(88)90101-5).
- Sheik, C.S., Badalamenti, J.P., Telling, J., Hsu, D., Alexander, S.C., Bond, D.R., Gralnick, J.A., Sherwood Lollar, B., Toner, B.M., 2021. Novel microbial groups drive productivity in an Archean iron formation. *Front. Microbiol.* 12 <https://doi.org/10.3389/fmicb.2021.627595>.
- Sherwood Lollar, B., Westgate, T.D., Ward, J.A., Slater, G.F., Lacrampe-Couloume, G., 2002. Abiogenic formation of alkanes in the earth's crust as a minor source for global hydrocarbon reservoirs. *Nature* 416, 522–524. <https://doi.org/10.1038/416522a>.
- Sherwood Lollar, B., Lacrampe-couloume, G., Slater, G.F., Ward, J., Moser, D.P., Gihring, T.M., Lin, L., Onstott, T.C., 2006. Unravelling Abiogenic and Biogenic Sources of Methane in the Earth's Deep Subsurface, 226, pp. 328–339. <https://doi.org/10.1016/j.chemgeo.2005.09.027>.
- Sherwood Lollar, B., Hirschorn, S.K., Chartrand, M.M.G., Lacrampe-Couloume, G., 2007. An approach for assessing total instrumental uncertainty in compound-specific carbon isotope analysis: implications for environmental remediation studies. *Anal. Chem.* 79, 3469–3475. <https://doi.org/10.1021/ac062299v>.
- Sherwood Lollar, B., Lacrampe-Couloume, G., Voglesonger, K., Onstott, T.C., Pratt, L.M., Slater, G.F., 2008. Isotopic signatures of  $\text{CH}_4$  and higher hydrocarbon gases from Precambrian Shield sites: a model for abiogenic polymerization of hydrocarbons. *Geochim. Cosmochim. Acta* 72, 4778–4795. <https://doi.org/10.1016/j.gca.2008.07.004>.
- Sherwood Lollar, B., Onstott, T.C., Lacrampe-Couloume, G., Ballentine, C.J., 2014. The contribution of the Precambrian continental lithosphere to global  $\text{H}_2$  production. *Nature* 516, 379–382. <https://doi.org/10.1038/nature14017>.
- Sherwood Lollar, B., Heuer, V.B., McDermott, J., Tille, S., Warr, O., Moran, J.J., Telling, J., Hinrichs, K.-U., 2021. A window into the abiotic carbon cycle – Acetate and formate in fracture waters in 2.7 billion year-old host rocks of the Canadian Shield. *Geochim. Cosmochim. Acta* 294, 295–314. <https://doi.org/10.1016/j.gca.2020.11.026>.
- Silver, B.J., Raymond, R., Sigman, D.M., Prokopenko, M., Sherwood Lollar, B., Lacrampe-couloume, G., Fogel, M.L., Pratt, L.M., Lefticariu, L., Onstott, T.C., 2012. The origin of  $\text{NO}_3$  and  $\text{N}_2$  in deep subsurface fracture water of South Africa. *Chem. Geol.* 294–295, 51–62. <https://doi.org/10.1016/j.chemgeo.2011.11.017>.
- Simkus, D.N., Slater, G.F., Lollar, B.S., Wilkie, K., Kieft, T.L., Magnabosco, C., Lau, M.C. Y., Pullin, M.J., Hendrickson, S.B., Wommack, K.E., Sakowski, E.G., Heerden, E. van, Kuloyo, O., Linage, B., Borgonie, G., Onstott, T.C., 2016. Variations in microbial carbon sources and cycling in the deep continental subsurface. *Geochim. Cosmochim. Acta* 173, 264–283. <https://doi.org/10.1016/j.gca.2015.10.003>.
- Sohlberg, E., Bomberg, M., Miettinen, H., Nyyssönen, M., Salavirta, H., Vikman, M., Itävaara, M., 2015. Revealing the unexplored fungal communities in deep groundwater of crystalline bedrock fracture zones in Olkiluoto. Finland. *Front. Microbiol.* 6, 573.
- Spinks, J.W.T., Woods, R.J., 1990. *An Introduction to Radiation Chemistry*, 3rd ed. John Wiley and Sons Inc.
- Stober, I., Bucher, K., 2007. Hydraulic properties of the crystalline basement. *Hydrogeol. J.* 15, 213–224.
- Takai, K., Moser, D.P., DeFlaun, M., Onstott, T.C., Fredrickson, J.K., 2001. Archaeal diversity in waters from Deep South African gold mines. *Appl. Environ. Microbiol.* 67, 5750–5760. <https://doi.org/10.1128/AEM.67.21.5750-5760.2001>.
- Telling, J., Voglesonger, K., Sutcliffe, C.N., Lacrampe-Couloume, G., Edwards, E., Sherwood Lollar, B., 2018. Bioenergetic constraints on microbial hydrogen utilization in precambrian deep crustal fracture fluids. *Geomicrobiol. J.* 35, 108–119. <https://doi.org/10.1080/01490451.2017.1333176>.
- Tolstikhin, I.N., et al., 2011. Production, redistribution and loss of helium and argon isotopes in a thick sedimentary aquitard– aquifer system (Molasse Basin, Switzerland). *Chem. Geol.* 286 (1–2), 48–58.
- Ward, J.A., Slater, G.F., Moser, D.P., Lin, L.H., Lacrampe-Couloume, G., Bonin, A.S., Davidson, M., Hall, J.A., Mislowski, B., Bellamy, R.E.S., Onstott, T.C., Sherwood Lollar, B., 2004. Microbial hydrocarbon gases in the Witwatersrand Basin, South Africa: Implications for the deep biosphere. *Geochim. Cosmochim. Acta* 68, 3239–3250. <https://doi.org/10.1016/j.gca.2004.02.020>.
- Warr, O., Sherwood Lollar, B., Fellowes, J., Sutcliffe, C.N., McDermott, J.M., Holland, G., Mabry, J.C., Ballentine, C.J., 2018. Tracing ancient hydrogeological fracture network age and compartmentalisation using noble gases. *Geochim. Cosmochim. Acta* 222, 340–362. <https://doi.org/10.1016/j.gca.2017.10.022>.
- Warr, O., Giunta, T., Ballentine, C.J., Sherwood Lollar, B., 2019. Mechanisms and rates of  $^4\text{He}$ ,  $^{40}\text{Ar}$ , and  $\text{H}_2$  production and accumulation in fracture fluids in Precambrian Shield environments. *Chem. Geol.* 530, 119322. <https://doi.org/10.1016/j.chemgeo.2019.119322>.
- Warr, O., Young, E.D., Giunta, T., Kohl, I.E., Ash, J.L., Sherwood Lollar, B., 2020. High-resolution, long-term isotopic and isotopologue variation identifies the sources and sinks of methane in a deep subsurface carbon cycle. *Geochim. Cosmochim. Acta* 294, 315–334. <https://doi.org/10.1016/j.gca.2020.12.002>.
- Warr, O., Giunta, T., Onstott, T.C., Kieft, T.L., Harris, R.L., Nisson, D.M., Sherwood Lollar, B., 2021. The role of low-temperature  $^{18}\text{O}$  exchange in the isotopic evolution of deep subsurface fluids. *Chem. Geol.* 561, 120027. <https://doi.org/10.1016/j.chemgeo.2020.120027>.
- Zinder, S.H., 1993. Physiological ecology of methanogens. In: *Methanogenesis*. Springer, pp. 128–206.